Geometry of thresholdless active flow in nematic microfluidics

Richard Green,[1] John Toner,[2,3] and Vincenzo Vitelli[1,4,*]
[1]*Instituut-Lorentz, Universiteit Leiden, 2300 RA Leiden, Netherlands*
[2]*Department of Physics and Institute of Theoretical Science, University of Oregon, Eugene, Oregon 97403, USA*
[3]*Max Planck Institute for the Physics of Complex Systems, Nöthnitzer Straße 38, 01187 Dresden, Germany*
[4]*The James Franck Institute and Department of Physics, The University of Chicago, Chicago, Illinois 60637, USA*
(Received 16 February 2016; revised manuscript received 11 January 2017; published 31 October 2017)

Active nematics are orientationally ordered but apolar fluids composed of interacting constituents individually powered by an internal source of energy. When activity exceeds a system-size-dependent threshold, spatially uniform active apolar fluids undergo a hydrodynamic instability leading to spontaneous macroscopic fluid flow. Here we show that a special class of spatially nonuniform configurations of such active apolar fluids display laminar (i.e., time-independent) flow even for arbitrarily small activity. We also show that two-dimensional active nematics confined on a surface of nonvanishing Gaussian curvature must necessarily experience a nonvanishing active force. This general conclusion follows from a key result of differential geometry: Geodesics must converge or diverge on surfaces with nonzero Gaussian curvature. We derive the conditions under which such curvature-induced active forces generate thresholdless flow for two-dimensional curved shells. We then extend our analysis to bulk systems and show how to induce thresholdless active flow by controlling the curvature of confining surfaces, external fields, or both. The resulting laminar flow fields are determined analytically in three experimentally realizable configurations that exemplify this general phenomenon: (i) toroidal shells with planar alignment, (ii) a cylinder with nonplanar boundary conditions, and (iii) a Frederiks cell that functions like a pump without moving parts. Our work suggests a robust design strategy for active microfluidic chips and could be tested with the recently discovered living liquid crystals.

DOI: 10.1103/PhysRevFluids.2.104201

I. INTRODUCTION

Active liquids [1] are complex fluids with some components individually capable of converting internal energy into sustained motion. These active components can be subcellular (such as microtubules powered by molecular motors, and actomyosin networks [2,3]), synthetic (e.g., self-propelled colloids [4] or interacting microrobots), or, alternatively, living organisms [5–8], such as birds, fish [9], microorganisms [10,11], or insects [12]. Hybrid systems composed of motile rod-shaped bacteria placed in nontoxic liquid crystals have also been realized recently [13]. All of these systems blur the line between the living and synthetic world, thereby opening up unprecedented opportunities for the design of novel smart materials and technology. At the same time, the far-from-equilibrium nature of active matter leads to exotic phenomena of fundamental interest. Among these are the ability of active fluids to (i) spontaneously break a continuous symmetry in two spatial dimensions [14–17], (ii) exhibit spontaneous steady-state flow [2,18] in the absence of an external driving force, and (iii) support topologically protected excitations (e.g., sound modes) that originate from time-reversal symmetry breaking [19].

A striking example of the phenomenon of spontaneous flow occurs in active nematic liquid crystals [1,18,20–24]. These materials are orientationally ordered but apolar fluids; that is, the active

*vitelli@uchicago.edu

particles share a common axis of motion but, in the homogeneous state, equal numbers of them move in each of the two directions parallel to this axis. As a result, there is no net motion and no net flow. However, if the activity parameter α (defined later) exceeds a critical threshold α_c, the undistorted nematic ground state becomes unstable. Once this instability threshold is passed, the active nematics spontaneously deform their state of alignment, triggering macroscopic turbulent flow [2,18,25–28]. For nematics, this activity threshold α_c goes to zero as the system size $L \to \infty$, $\alpha_c \sim \frac{K}{L^2}$, where K is a characteristic Frank elastic constant. Equivalently, one can say that the instability-triggered flow does not occur in systems of characteristic size smaller than $L_{\text{inst}} \sim \sqrt{\frac{K}{|\alpha|}}$.

In this paper we describe conditions for active flow that may be realized for systems with length scales less than L_{inst}, which also corresponds to the limit of small activity. Numerical studies of active nematics suggest that some nonuniform director configurations can lead to laminar flow for arbitrarily small activity, i.e., well below the instability threshold [25]. However, no systematic study of the mechanisms and criteria behind such thresholdless active flow has previously been undertaken. In this paper we use a well-established hydrodynamic theory of active nematics to identify the class of surface deformations, boundary conditions, or external fields that induce a nonuniform director ground state capable of generating such thresholdless laminar flow. We emphasize that not all spatially nonuniform configurations will induce such flow.

The condition for a given set of boundary conditions and applied fields to induce thresholdless active flow in nematics is most easily expressed in terms of the director field $\hat{\boldsymbol{n}}(\boldsymbol{r})$ [29], which is defined as the local orientation of molecular alignment. It can be stated as follows: If the active force, which is

$$\boldsymbol{f}_a \equiv \alpha[\hat{\boldsymbol{n}}(\nabla \cdot \hat{\boldsymbol{n}}) + (\hat{\boldsymbol{n}} \cdot \nabla)\hat{\boldsymbol{n}}] = \alpha[\hat{\boldsymbol{n}}\nabla \cdot \hat{\boldsymbol{n}} - \hat{\boldsymbol{n}} \times (\nabla \times \hat{\boldsymbol{n}})], \tag{1}$$

has nonzero curl, when computed for the director configuration $\hat{\boldsymbol{n}}(\boldsymbol{r})$ that minimizes the Frank elastic free energy (including external fields) of the corresponding equilibrium problem [29], then the active fluid in the same geometry must flow (i.e., the velocity field $\boldsymbol{v} \neq \boldsymbol{0}$). Note that this condition is far more stringent than simply requiring that the nematic ground-state orientation be inhomogeneous. For example, any pure twist configuration (e.g, a cholesteric, or a twist cell) does not satisfy it, since splay $\nabla \cdot \hat{\boldsymbol{n}}$ and bend $\hat{\boldsymbol{n}} \times (\nabla \times \hat{\boldsymbol{n}})$ both vanish in such configurations. Note that the criterion $\nabla \times \boldsymbol{f}_a \neq \boldsymbol{0}$ is a sufficient condition for thresholdless flow.

In the present study we calculate the resulting flow field $\boldsymbol{v}(\boldsymbol{r})$ explicitly in the frozen director approximation, in which the nematic director remains in its equilibrium configuration when activity is turned on. We consider this regime mainly to derive analytical solutions and provide qualitative insights into the nature of the flow, but it has in fact been realized experimentally in living liquid crystals [30]. We also demonstrate that this approximation is asymptotically exact in the experimentally relevant limit of weak orientational order. Since many nematic to isotropic transitions are weakly first order [29] (at least in equilibrium), this frozen director limit may be realized close to such transitions. Moreover, these solutions provide qualitative insights into the nature of the flow even in systems in which the frozen director approximation is not quantitatively accurate. Our ideas can also be applied with some modifications to the recently discovered living liquid crystals [13]. These systems are a mixture of two components: living bacteria, which provide the activity, and a background medium composed of nematically ordered nonactive molecules. On symmetry grounds, as we discuss in more detail in Appendix I, these systems considered in their entirety are active nematics.

The remainder of this paper is organized as follows. In Sec. II we introduce the simplified model for the hydrodynamics of active nematics adopted in our study. We also discuss some generalizations of this model and argue that none of our conclusions will be substantively affected by these generalizations. In Sec. III we derive the general criterion for thresholdless active flow. In Sec. IV we apply this criterion to the specific case of surfaces of nonzero Gaussian curvature and show that such surfaces always have nonzero active forces, but need not always have thresholdless flow. We also derive the additional criteria that must be satisfied for thresholdless flow to occur in these systems, give a specific example (active nematics on a thin toroidal shell) in which these

conditions are met, and work out the flow field in this case. In Sec. V we derive similar results for bulk systems with curved boundaries. Section VI presents calculations, in the frozen director approximation, of the flow fields that result in microchannels with prescribed anchoring angles on the surface and Sec. VII presents a design for an active pump in which a Frederiks cell geometry is used to switch on thresholdless active flow. We summarize in Sec. VIII.

II. HYDRODYNAMICS OF ACTIVE NEMATICS

We take as our model for an incompressible, one-component active nematic fluid the following three coupled equations [18]:

$$\rho_0 \frac{Dv_k}{Dt} = -\partial_k P + \eta \nabla^2 v_k + \alpha \partial_j (n_j n_k) + \partial_j \left(\lambda_{ijk} \frac{\delta F}{\delta n_i} \right), \tag{2a}$$

$$\frac{Dn_i}{Dt} = \lambda_{ijk} \partial_j v_k - \frac{1}{\gamma_1} \left[\frac{\delta F}{\delta n_i} - \left(\frac{\delta F}{\delta n_j} n_j \right) n_i \right], \tag{2b}$$

$$\boldsymbol{\nabla} \cdot \boldsymbol{v} = 0, \tag{2c}$$

where $D/Dt \equiv \partial_t + \boldsymbol{v} \cdot \boldsymbol{\nabla}$ is the convective derivative and the tensor λ_{ijk} reads

$$\lambda_{ijk} \equiv \left(\frac{\lambda + 1}{2} \right) n_j \delta_{ik} + \left(\frac{\lambda - 1}{2} \right) n_k \delta_{ij} - \lambda n_i n_j n_k. \tag{3}$$

Equation (2a) is a modified Navier-Stokes equation describing the evolution of the velocity field $\boldsymbol{v}(\boldsymbol{r},t)$; Eq. (2b) is the nematodynamic equation describing the evolution of the director field $\hat{\boldsymbol{n}}(\boldsymbol{r},t)$, which responds both to the flow $\boldsymbol{v}$ and to its own molecular field $\frac{\delta F}{\delta \boldsymbol{n}}$ (described in more detail below); and (2c) is the incompressibility condition, which is required since we take the density ρ_0 to be constant. We denote by P the dynamic pressure, by η the shear viscosity, which we take to be isotropic for simplicity, and by γ_1 the director field rotational viscosity. The dimensionless flow-alignment parameter λ captures the anisotropic response of the nematogens to shear. Note that the key difference between Eqs. (2a)–(2c) and the equations of motion for an equilibrium nematic [29] is the active force term $\alpha \partial_j (n_j n_k)$ in the Navier-Stokes equation (2a), which may be contractile ($\alpha > 0$) or extensile ($\alpha < 0$), depending on the system [18]. The molecular field $\frac{\delta F}{\delta \boldsymbol{n}}$, derived from the Frank free energy

$$F = \frac{1}{2} \int d^3 r \{ K_1 (\boldsymbol{\nabla} \cdot \hat{\boldsymbol{n}})^2 + K_2 [\hat{\boldsymbol{n}} \cdot (\boldsymbol{\nabla} \times \hat{\boldsymbol{n}})]^2 + K_3 |\hat{\boldsymbol{n}} \times (\boldsymbol{\nabla} \times \hat{\boldsymbol{n}})|^2 \}, \tag{4}$$

is parametrized respectively by three independent elastic constants $K_{1,2,3}$ for splay, twist, and bend deformations of the director.

Many experimental realizations of active nematics, such as the living liquid crystals [13], are multicomponent systems. This leads to several differences between their hydrodynamic theories and that embodied by Eqs. (2a)–(2c); in particular, the concentration of each additional component must be added as a new hydrodynamic variable. However, the resulting hydrodynamic equations are sufficiently similar to the one-component case we consider here that our criteria for thresholdless flow remain valid; a demonstration of this is beyond the scope of the present paper. We discuss the applicability of a multicomponent generalization of the hydrodynamic equations presented here to living liquid crystals in Appendix I.

We also note that, strictly speaking, Eqs. (2a)–(2c) are not the most general set of equations for a one-component active nematic. Specifically, there are two ways in which they could be generalized.

(i) The free energy F that appears in the velocity equation of motion (2a) need not, in a nonequilibrium system, be the same as that in the director equation of motion (2b). Both free energies have to have the same form as (4), since that form is required by rotation invariance, but the Frank constants $K_{1,2,3}$ that appear in them need not be equal.

(ii) The viscosity need not be isotropic: There are in general six Leslie coefficients [31] characterizing this anisotropic response.

In Appendix A we show that, for small activity, the former effect is negligible: The Frank constants in the velocity equation of motion (2a) approach those in the director equation of motion (2b) as activity goes to zero. Hence, since we are interested here in the limit of small activity, this difference becomes negligible. Furthermore, for weak orientational order, our approximation of isotropic viscosity becomes asymptotically exact. Indeed, Kuzuu and Doi [32] showed that the anisotropic parts of the viscosities vanish as the amplitude of the nematic order parameter goes to zero (the isotropic viscosity does not vanish in the same limit since a completely isotropic liquid has a nonvanishing isotropic viscosity). To sum up, the hydrodynamic theory we employ is exact for low-activity, weakly ordered nematics.

Most of our conclusions are independent of this limit; in particular, our criteria for thresholdless active flow are dictated only by the form of the active force $\boldsymbol{f}_a$, which is unchanged by making the viscosity tensor anisotropic and is furthermore independent of the assumption that the two Frank energies F_n and F_v are the same.

III. THRESHOLDLESS FLOW IN ACTIVE NEMATICS

At the heart of our study lies a simple observation: The constitutive equations (2a)–(2c) of active nematics inevitably imply that, in certain geometries, an arbitrarily small activity induces steady-state macroscopic fluid flow. We will prove this by contradiction. If there is no fluid flow (i.e., if the velocity field $\boldsymbol{v} = \boldsymbol{0}$), then the equation of motion (2b) for the director field implies that, in a steady state, for which $\frac{Dn_i}{Dt} = 0$, $\frac{\delta F}{\delta \boldsymbol{n}} - (\hat{\boldsymbol{n}} \cdot \frac{\delta F}{\delta \boldsymbol{n}})\hat{\boldsymbol{n}} = \boldsymbol{0}$ (which also holds in the case of anisotropic viscosity). This is simply the Euler-Lagrange equation for minimizing the Frank free energy F subject to the constraint $|\hat{\boldsymbol{n}}| = 1$. The contradiction arises when we insert such an equilibrium solution for the nematic director into the equation of motion for the velocity field (2a).

The last term on the right-hand side of Eq. (2a), involving $\frac{\delta F}{\delta \boldsymbol{n}}$, vanishes when $\frac{\delta F}{\delta \boldsymbol{n}} \parallel \hat{\boldsymbol{n}}$, which is the case when the director field is in its ground state. Since the velocity field $\boldsymbol{v}$ vanishes, Eq. (2a) reduces to $\nabla P = \alpha(\hat{\boldsymbol{n}} \cdot \nabla \hat{\boldsymbol{n}} + \hat{\boldsymbol{n}} \nabla \cdot \hat{\boldsymbol{n}}) \equiv \boldsymbol{f}_a$. Hence the pressure gradient must cancel the active force to prevent flow, but this is not possible if the active force has a nonvanishing curl. In such cases, $\boldsymbol{v} = \boldsymbol{0}$ can never be a solution in the presence of activity; the fluid must flow, no matter how small the activity. Thus, a sufficient condition for thresholdless active flow is

$$\nabla \times \boldsymbol{f}_a \neq \boldsymbol{0}, \tag{5}$$

which has also been implicit in other work such as [33].

One class of director configurations for which the condition in Eq. (5) is not satisfied is that of pure twist configurations, that is, configurations in which the twist does not vanish [i.e., $\hat{\boldsymbol{n}} \cdot (\nabla \times \hat{\boldsymbol{n}}) \neq 0$], but the splay and bend do [i.e., $\nabla \cdot \hat{\boldsymbol{n}} = 0$ and $\hat{\boldsymbol{n}} \times (\nabla \times \hat{\boldsymbol{n}}) = \boldsymbol{0}$, respectively]. This can be seen by using the vector calculus identity $[\hat{\boldsymbol{n}} \times (\nabla \times \hat{\boldsymbol{n}})]_i = n_j \nabla_i n_j - \hat{\boldsymbol{n}} \cdot \nabla n_i = \frac{1}{2}\nabla_i |\hat{n}|^2 - \hat{\boldsymbol{n}} \cdot \nabla n_i = -\hat{\boldsymbol{n}} \cdot \nabla n_i$, where in the last equality we have used the fact that $\hat{\boldsymbol{n}}$ is a unit vector to set $\nabla_i |\hat{n}|^2 = \nabla_i 1 = 0$. Using this, the active force $\boldsymbol{f}_a$ may be rewritten as

$$\boldsymbol{f}_a = \alpha[\hat{\boldsymbol{n}} \nabla \cdot \hat{\boldsymbol{n}} - \hat{\boldsymbol{n}} \times (\nabla \times \hat{\boldsymbol{n}})], \tag{6}$$

which implies that a director field with pure twist has zero active force and hence no flow for sufficiently small activity.

When we consider specific examples of thresholdless active flow in the remainder of this paper, we will determine analytically the velocity field $\boldsymbol{v}(\boldsymbol{r},t)$. In general, this is a difficult nonlinear calculation, since the flow field reorients the nematic director. However, in the frozen director limit $\gamma_1 \ll \eta$, turning on activity (and thereby inducing thresholdless flow) does not lead to an appreciable change in the nematic director configuration from that in equilibrium, which is obtained by minimizing the Frank free energy. We show in Appendix B that there is a very natural, generic, and well-defined limit in which γ_1 will always be much less than η, namely, the limit of weak nematic

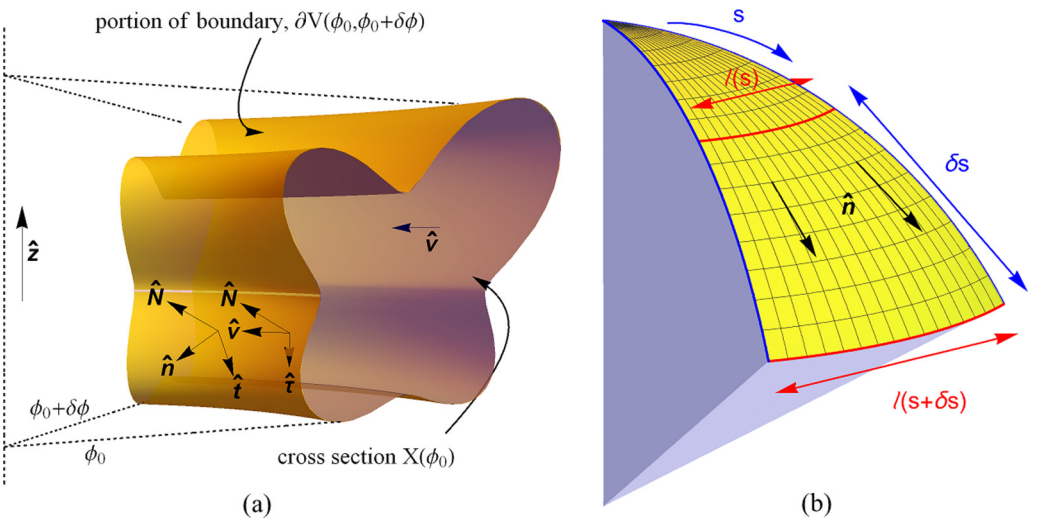

FIG. 1. (a) Volume V' of arbitrary cross section with torsional symmetry. The normal to the bounding surface is $\hat{\boldsymbol{N}}$ and two orthonormal sets of unit vectors are shown: (i) director field $\hat{\boldsymbol{n}}$ tangential to the bounding surface with $\hat{\boldsymbol{t}} = \hat{\boldsymbol{N}} \times \hat{\boldsymbol{n}}$ and (ii) direction of symmetry $\hat{\boldsymbol{v}}$ also tangential to bounding surface with $\hat{\boldsymbol{\tau}} = \hat{\boldsymbol{N}} \times \hat{\boldsymbol{v}}$. (b) Distance between geodesics $\ell(s)$ as a function of the arc length s in the case of planar anchoring of the director $\hat{\boldsymbol{n}}$ on a surface with Gaussian curvature.

order. Although we initially conceived the frozen director regime for calculational convenience to derive analytical expressions for the flow, this regime has in fact been realized experimentally in living liquid crystal systems in which bacteria are subjected to a preimposed director field that is effectively frozen in the experiment [30].

IV. TWO-DIMENSIONAL CURVED SYSTEMS

A. General considerations

Consider an active nematic material confined to a curved monolayer shell, such as that shown in Fig. 1. Such systems are of special interest since many active nematics synthesized to date are monolayers or thin shells with planar anchoring [20,23]. In this section we will show that, in general, a shell with nonvanishing Gaussian curvature G generates a nonvanishing active force $\boldsymbol{f}_a$. To prove this result, we first assume that, if the shell is very thin, the component of $\hat{\boldsymbol{n}}$ perpendicular to the surface is negligible everywhere inside the shell [34–36], i.e., planar anchoring conditions. In this case, we can decompose the active force $\boldsymbol{f}_a(\boldsymbol{x})$ at position $\boldsymbol{x}$ along three orthogonal directions: (i) the local surface normal $\hat{\boldsymbol{N}}$, (ii) the nematic director $\hat{\boldsymbol{n}}$, and (iii) the tangent vector $\hat{\boldsymbol{t}}$ perpendicular to both $\hat{\boldsymbol{N}}$ and $\hat{\boldsymbol{n}}$, shown in Fig. 1(a) [which in addition shows a second orthonormal set of unit vectors $(\hat{\boldsymbol{N}}, \hat{\boldsymbol{v}}, \hat{\boldsymbol{\tau}})$ used below in Sec. V]. The active force reads

$$\boldsymbol{f}_a(\boldsymbol{x}) = \alpha[\hat{\boldsymbol{n}}(\boldsymbol{x})\nabla \cdot \hat{\boldsymbol{n}}(\boldsymbol{x}) + \hat{\boldsymbol{t}}(\boldsymbol{x})\kappa_g(\boldsymbol{x}) + \hat{\boldsymbol{N}}(\boldsymbol{x})\kappa_n(\boldsymbol{x})], \tag{7}$$

where $\kappa_n = \hat{\boldsymbol{N}} \cdot (\hat{\boldsymbol{n}} \cdot \nabla)\hat{\boldsymbol{n}}$ defines the local normal curvature of the nematic director field $\hat{\boldsymbol{n}}(\boldsymbol{x})$ and $\kappa_g = \hat{\boldsymbol{t}} \cdot (\hat{\boldsymbol{n}} \cdot \nabla)\hat{\boldsymbol{n}}$ defines its geodesic curvature [37,38], which quantifies deviations from the local geodesic tangent to $\hat{\boldsymbol{n}}$. In particular, it is a theorem of differential geometry [37] that, if $\kappa_g = 0$ for the director field lines everywhere, the nematic director must lie on geodesics.

Since the set of vectors $(\hat{\boldsymbol{N}}, \hat{\boldsymbol{n}}, \hat{\boldsymbol{t}})$ is orthonormal, the active force can only vanish if all three of its components vanish. In particular, this implies that $\kappa_g = 0$. However, we now show that the condition $\kappa_g = 0$ forces the $\hat{\boldsymbol{n}}$ component of $\boldsymbol{f}_a$ (which is proportional to $\nabla \cdot \hat{\boldsymbol{n}}$) to be nonzero, on any surface with nonzero Gaussian curvature. To prove this statement, note that if $\kappa_g = 0$, the nematic director

must lie on geodesics everywhere on the surface, as illustrated in Fig. 1(b). Consider an infinitesimal patch bounded by two geodesics (along which the nematic director is aligned) and their normals, shown in Fig. 1(b). These perpendicular arcs have length equal to the distance $\ell(s)$ between the two geodesics parametrized by the arc length s along one of them. We now apply the divergence theorem to the director field $\hat{\boldsymbol{n}}$ on this small patch, whose area is approximately given by ds times $\ell(s)$. The $\hat{\boldsymbol{n}}$ flux vanishes along the two geodesics and is equal to $\ell(s+ds)$ and $-\ell(s)$ along the two normal arcs, which yields

$$\boldsymbol{\nabla}\cdot\hat{\boldsymbol{n}} = \frac{1}{\ell}\frac{d\ell}{ds}. \tag{8}$$

The right-hand side of Eq. (8) cannot be identically zero because $\frac{d^2\ell}{ds^2} = -G(\boldsymbol{x})\ell$ on an arbitrary surface with nonvanishing $G(\boldsymbol{x})$ [39]. Intuitively, Gaussian curvature forces geodesics to either converge or diverge, which in turn implies that $\boldsymbol{\nabla}\cdot\hat{\boldsymbol{n}} \neq 0$. The converse statement also holds, namely, that $\boldsymbol{\nabla}\cdot\hat{\boldsymbol{n}} = 0$ requires $\kappa_g \neq 0$. Thus we have proved that nonvanishing Gaussian curvature G implies a nonvanishing active force $\boldsymbol{f}_a$. The incompatibility relation derived above has a purely geometric origin and it is also responsible for the geometric frustration of nematic (and more generally orientational and crystalline) order in curved space. This general result is independent of specific choices of elastic constants and other material parameters, such as the viscosity tensor.

We can therefore state the sufficient condition for thresholdless flow

$$G(\boldsymbol{x}) \neq 0 \tag{9}$$

at some point $\boldsymbol{x}$ on the shell and

$$\oint_C d\boldsymbol{l}\cdot\boldsymbol{f}_a \neq 0 \tag{10}$$

for some closed loop C on the shell. As we have argued above, Eq. (9) guarantees that $\boldsymbol{f}_a \neq 0$ and Eq. (10) implies that $\boldsymbol{f}_a$ cannot be balanced by $\boldsymbol{\nabla}P$, since $\boldsymbol{\nabla}P$ is by definition a conservative force. Thus, if the conditions (9) and (10) are satisfied, there must be flow.

Our derivation of this condition never assumed that the director configuration was free of topological defects (i.e., disclinations); hence the active force must be nonzero for any surface with nonvanishing Gaussian curvature, even if, as often happens [40,41], that Gaussian curvature induces disclinations on the surface. Indeed, topological defects, far from preventing flow, probably make it inevitable (a result first noted in Refs. [21,22] for flat surfaces), since they induce large director gradients near their core. Note, however, that the condition (10) will not be satisfied in general for all surfaces with nonzero Gaussian curvature. In the next section, we consider a specific example that illustrates this point.

B. Chiral symmetry breaking and flow in toroidal shells

Let us focus our analysis on the case of a curved nematic monolayer with the molecules aligned tangent to the surface of a torus, but free to determine their local in-plane orientation. Since the torus is a surface of nonzero Gaussian curvature, there must be a nonvanishing active force based on our previous reasoning. We now demonstrate that, as the aspect ratio of the torus is changed, this active force results in no net flow for very slender tori (which are nearly cylinders), while for fatter tori, there is a transition to a chiral director configuration in which the active force does have a nonzero line integral. Hence, by the criteria of the preceding section, flow must ensue. We compute such flow in the aforementioned frozen director approximation.

Consider the set of toroidal coordinates (ρ,ϕ,ψ) shown in Fig. 2(a), where ρ is the dimensionless radial coordinate set to 1 on the monolayer surface, ψ is the poloidal angle, and ϕ is the toroidal or azimuthal angle. The slenderness of the torus $\xi \equiv R_1/R_2$ is the aspect ratio of its major (R_1) and minor (R_2) radii. On the thin toroidal shell we are considering here, $\rho \equiv r/R_2$ takes values $1-\delta \leqslant \rho \leqslant 1$ with $\delta \ll 1$. For very slender tori (which are nearly cylinders), the nematic director

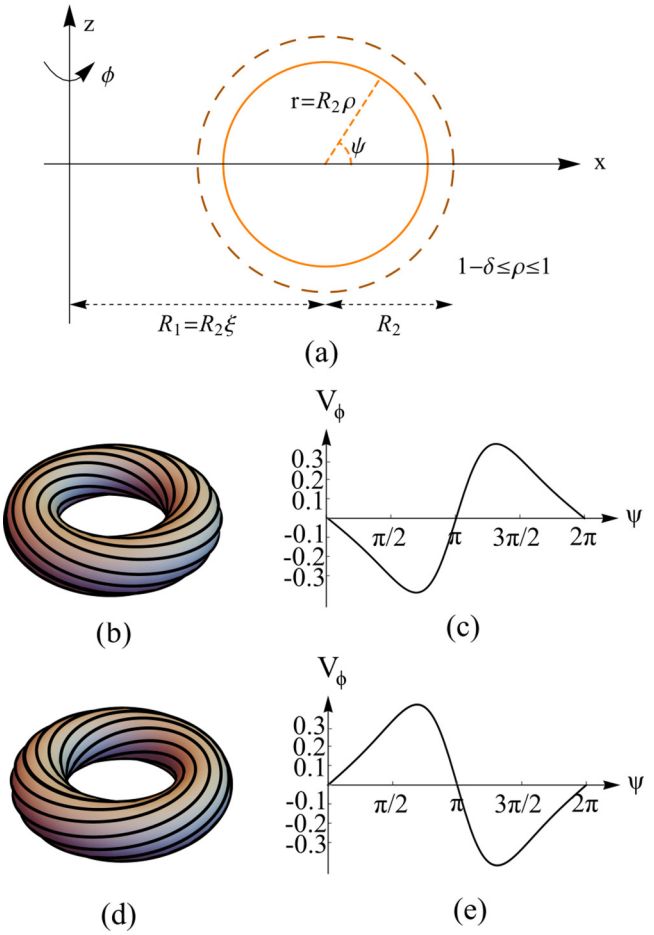

FIG. 2. (a) Toroidal coordinates. The plane $y = 0$ is shown for the $x \geqslant 0$ half of the toroid using (ρ,ϕ,ψ) coordinates where ϕ is the azimuthal angle and ψ the poloidal angle. Here $R_{1,2}$ are the major and minor radii, respectively, of the torus; $\rho \equiv r/R_2$ takes values $1 - \delta \leqslant \rho \leqslant 1$ with $\delta \ll 1$ for a thin shell. (b) Nematic director field lines for the left chiral ground state ($\omega < 0$). (c) Plot of the magnitude of the velocity in the $\hat{\boldsymbol{\phi}}$ direction versus ψ. (d) Nematic director field lines for the right chiral ground state ($\omega > 0$). (e) Plot of the magnitude of the velocity in the $\hat{\boldsymbol{\phi}}$ direction versus ψ. Activity is extensile ($\alpha < 0$) and in (c) and (e), the speed is measured in units of $|\alpha\omega|/\gamma R_2$ (see the text).

will be everywhere oriented along $\hat{\boldsymbol{\phi}}$. This bend-only configuration is divergenceless, hence the first term of Eq. (7) is zero. Note, however, that κ_g will be different from zero because the nematic director lines are not geodesics. In fact, $\kappa_g = \sin\psi/R_2(\xi + \cos\psi)$ and $\kappa_n = -\cos\psi/R_2(\xi + \cos\psi)$, so in this case $\boldsymbol{f}_a = -\alpha\nabla\ln(\xi + \rho\cos\psi)$. The condition (10) is not satisfied and there is no flow because the active force is completely balanced by the pressure gradient.

For sufficiently fat (i.e., small ξ) tori, this uniform azimuthal director state becomes unstable to one that has nonzero twist. We extend the approach used in Refs. [42–44] to a two-dimensional curved monolayer by considering the following variational ansatz which captures the qualitative features of the chiral symmetry-breaking transition in the ground state at zero activity:

$$\hat{\boldsymbol{n}} = \frac{\omega\xi}{\xi + \cos\psi}\hat{\boldsymbol{\psi}} + \sqrt{1 - \left(\frac{\omega\xi}{\xi + \cos\psi}\right)^2}\,\hat{\boldsymbol{\phi}}, \tag{11}$$

where ω is a variational parameter describing the degree of twist in the director field.

In Appendix E we show that to leading order in $1/\xi$, the two ground states in Figs. 2(b) and 2(d) correspond to

$$\omega = \pm\sqrt{\frac{5}{4\xi^2} - \frac{K_2}{2K_3}}, \tag{12}$$

provided that the quantity under the square root is positive (otherwise the ground state is the untwisted state $\omega = 0$). To $O(\omega)$, the corresponding active force, evaluated on the surface of the torus (i.e., $\rho = 1$), reads

$$\boldsymbol{f}_a = \frac{-\alpha\left(\hat{\boldsymbol{\rho}}\cos\psi - \hat{\boldsymbol{\psi}}\sin\psi + \hat{\boldsymbol{\phi}}\frac{\omega\xi\sin\psi}{\xi+\cos\psi}\right)}{R_2(\xi+\cos\psi)}. \tag{13}$$

The condition (10) is now satisfied by a closed loop C everywhere in the $\hat{\boldsymbol{\phi}}$ direction and so we conclude that there must be thresholdless flow. In a two-dimensional nematic shell draped on a substrate, momentum is not generally conserved; therefore, a frictional term $-\gamma v_k$ must be added to the right-hand side of Eq. (2a). (In general, γ will be a second-rank tensor, but we ignore this effect in our simplified treatment.) In the limit $\gamma \gg \eta/L^2$, where L is the size of the sample, this frictional drag dominates the viscous forces and the revised form of Eq. (2a) reads

$$\nabla P + \gamma \boldsymbol{v} = \boldsymbol{f}_a. \tag{14}$$

Taking the divergence of Eq. (13), we see that Eq. (14) can be solved to obtain the pressure $P = -\alpha\ln(\xi+\rho\cos\psi)$. Therefore, on the shell where $\rho = 1$, the velocity is given by

$$\boldsymbol{v} = \frac{-\alpha}{\gamma R_2}\frac{\omega\xi\sin\psi}{(\xi+\cos\psi)^2}\hat{\boldsymbol{\phi}} + O(\omega^2). \tag{15}$$

This solution is a flow one way in the $\hat{\boldsymbol{\phi}}$ direction on the top half of the toroidal shell and in the opposite direction on the bottom half. The orientation of the flow is determined by the sign of the activity (contractile or extensile) and the chirality of the ground state, as illustrated in Fig. 2.

In the above analysis, we used a smooth, defect-free toroidal ansatz (11), which explicitly excludes the possibility of topological defects in the nematic director configuration. This is valid in the limit of high slenderness ξ, in which the Gaussian curvature is too small to induce defects [40]. However, as we have noted above, defects make flow inevitable, since they induce large director gradients near themselves. Therefore, by excluding such defects, we have actually maximized the chance of having no thresholdless flow. We therefore conclude that for tori fatter than $\xi < \xi_c = \sqrt{\frac{5K_3}{2K_2}}$ (the last equality holding approximately when $K_3 \gg K_2$), thresholdless active flow will definitely occur. If disclinations are not generated and the aforementioned conditions for the validity of the frozen director approximation hold, then the flow field should be approximately described by our result (15).

In Appendix F we solve the three-dimensional (3D) bulk version of this toroidal system with no-slip boundary conditions. This is a more complicated calculation, as Eq. (14) becomes $\nabla P - \eta\nabla^2\boldsymbol{v} = \boldsymbol{f}_a$, which must be solved in the bulk toroidal geometry, but the general features of the solution are similar to the shell case.

V. THREE-DIMENSIONAL SYSTEMS WITH CURVED BOUNDARIES

We now turn to investigate how the geometry of the boundaries and anchoring conditions of the director can also force thresholdless flow in bulk active nematics under confinement. This may be of practical importance, since controlling boundaries and boundary conditions for liquid crystals is a highly developed technology that has long been used for the construction of liquid crystal displays. Efforts are under way to extend such control to the active regime [13,45,46].

Consider nonplanar alignment of the director to the walls of a three-dimensional channel with torsional symmetry [by which we mean equivalently that the sample is bounded by a surface of revolution about the z axis as shown in Fig. 1(a)]. The nematic liquid crystal fills the bulk bounded by the surface. If we make the additional assumption that the pressure gradient vanishes along the direction of torsional symmetry, which we denote by $\hat{\boldsymbol{v}}$, a nonzero component of the active force along $\hat{\boldsymbol{v}}$ will result in thresholdless flow.

A small section of a channel V' bounded by an arbitrarily shaped surface with torsional symmetry along $\hat{\boldsymbol{v}}$ is shown in Fig. 1(a), where the local surface normal is represented by the unit vector $\hat{\boldsymbol{N}}(\boldsymbol{x})$. Denoting the torsional coordinate by ϕ, the volume V' is the section of the three-dimensional channel bounded by the surfaces $\phi = \phi_0$ and $\phi = \phi_0 + \delta\phi$. The integrated force $\boldsymbol{F}(\phi_0)$ acting on the volume V' can then be obtained by integrating the force density $(f_a)_i = \alpha\partial_j(n_i n_j)$ over the infinitesimal volume V'. Applying the divergence theorem, we obtain the projection of $\boldsymbol{F}(\phi_0)$ along $\hat{\boldsymbol{v}}(\phi_0)$ in terms of the anchoring conditions of the nematic director at the boundary, leading to the sufficient condition for thresholdless flow

$$0 \neq \boldsymbol{F}(\phi_0)\cdot\hat{\boldsymbol{v}}(\phi_0) = \alpha \iint\limits_{\partial V(\phi_0,\phi_0+\delta\phi)} dS(\hat{\boldsymbol{N}}\cdot\hat{\boldsymbol{n}})(\hat{\boldsymbol{v}}\cdot\hat{\boldsymbol{n}}) + \alpha\delta\phi \iint\limits_{X(\phi_0)} dS(\hat{\boldsymbol{v}}\times\hat{\boldsymbol{z}}\cdot\hat{\boldsymbol{n}})(\hat{\boldsymbol{v}}\cdot\hat{\boldsymbol{n}}), \tag{16}$$

where $\hat{\boldsymbol{z}}$ is the axis of torsional symmetry [see Fig. 1(a)], so that in cylindrical coordinates centered on the axis of symmetry, $\hat{\boldsymbol{v}}\times\hat{\boldsymbol{z}}$ is a unit vector in the radial direction. A detailed derivation of Eq. (16) in the case of general curvilinear coordinates under suitable assumptions is provided in Appendix C. Here we note that in the case of a sample with high slenderness (for which the radius of curvature along $\hat{\boldsymbol{v}}$ is much greater than in the directions perpendicular to it), the second term may be dropped relative to the first term. Once this simplification is made, the condition (16) becomes

$$0 \neq \boldsymbol{F}(\phi_0)\cdot\hat{\boldsymbol{v}}(\phi_0) = \alpha \iint\limits_{\partial V(\phi_0,\phi_0+\delta\phi)} dS(\hat{\boldsymbol{N}}\cdot\hat{\boldsymbol{n}})(\hat{\boldsymbol{v}}\cdot\hat{\boldsymbol{n}}), \tag{17}$$

which we see is met as long as the nematic director $\hat{\boldsymbol{n}}$ is not perpendicular to $\hat{\boldsymbol{N}}$ or $\hat{\boldsymbol{v}}$ on all the surfaces bounding the volume element.

To illustrate this criterion with an example, consider an active nematic confined between two infinite parallel plates, one with perpendicular and the other with planar anchoring, shown in Fig. 3. The director field and flow profile for this system were determined numerically in Ref. [25] and are calculated approximately in Appendix G. Here we deduce the main features of the flow using simple geometric arguments without carrying out explicit calculations. First, notice that because of the symmetry in the y direction, this system is the high slenderness limit of a similar torsionally symmetric system. This can be seen by giving the system torsional symmetry by revolving the figure about, say, the point $(-R,0)$ in the (x,y) plane to create an annulus. The high slenderness limit is obtained by sending $R\to\infty$ and recovering Fig. 3, in which case Eq. (17) is exact. However, $\boldsymbol{F}\cdot\hat{\boldsymbol{v}} = 0$ in this cell because $\hat{\boldsymbol{N}}\cdot\hat{\boldsymbol{n}} = 0$ on one plate and $\hat{\boldsymbol{v}}\cdot\hat{\boldsymbol{n}} = 0$ on the other. Nonetheless, active nematics flow at arbitrary small α in such a mixed alignment cell. This can be explained by applying Eq. (17) to either of the two portions of the cell, on opposite sides of the plane (parallel to both walls), whose surface normal $\hat{\boldsymbol{N}}$ makes an angle of $\pi/4$ with $\hat{\boldsymbol{n}}$. The boundary conditions on $\hat{\boldsymbol{n}}$, and continuity, ensure that such a plane exists, though it will not, for arbitrary and unequal values of the Frank constants $K_{1,2,3}$, be the midplane. According to Eq. (17), the resulting active forces in each of the two portions will be nonzero but of opposite sign; hence, the two sides must flow in opposite directions. In the special case of equal Frank constants $K_1 = K_2 = K_3$, the midplane is the plane on which the surface normal $\hat{\boldsymbol{N}}$ makes an angle of $\pi/4$ with $\hat{\boldsymbol{n}}$ and the flow in the two halves cancels out, leading to zero net flow in the whole cell. In the generic case of unequal Frank constants, this cancellation does not occur, leading to nonzero net flow, as discussed in Appendix G.

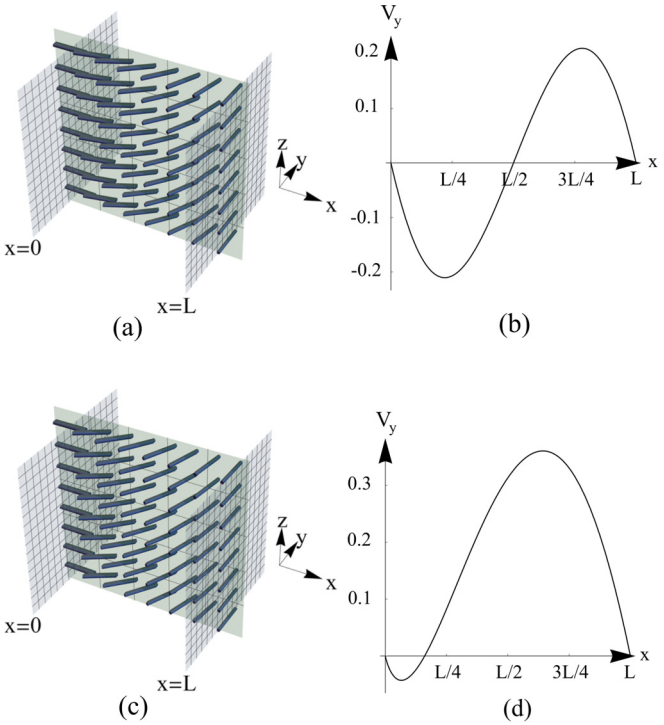

FIG. 3. Nematic director field ground state and associated flow generated with mixed boundary conditions in two dimensions. (a) Director field in the isotropic case $K_1 = K_3$ and (b) associated plot of the magnitude of the velocity v_y versus x. (c) Director field in the anisotropic case $K_1 \gg K_3$ and (d) associated plot of the magnitude of the velocity v_y versus x. The director field is represented by dark blue rods and the velocity is measured in units of $|\alpha|L/2\pi\eta$, with extensile activity ($\alpha < 0$). Movies are available in the Supplemental Material [47].

VI. FLOW IN MICROCHANNELS WITH PRESCRIBED ANCHORING ANGLE

We now illustrate this criterion for thresholdless active flow in three dimensions with the simple case of an infinite cylindrical channel with a nematic director field anchored on its boundary at a fixed angle Φ_0 to the axis of the cylinder, as shown in Fig. 4. Taking the usual cylindrical coordinates (ρ,θ,z), there is full symmetry in the θ direction as well as the z direction (which we also take to be the direction of symmetry $\hat{\mathbf{v}}$ of Sec. IV). Furthermore, since the cylinder can be thought of as an infinitely slender torus, again Eq. (17) is exact.

Even if $\Phi_0 = \pi/2$ (homeotropic anchoring), the nematic director configuration that minimizes the Frank free energy gradually escapes into the third dimension [48,49], becoming aligned with the $\hat{\mathbf{v}}$ axis at the center of the cylinder, as shown in Fig. 4. Consider now a different volume, enclosed on the outside by the outer boundary in Fig. 4 and on the inside by a concentric inner cylinder, so that $\hat{\boldsymbol{N}}$ and $\hat{\mathbf{v}}$ are aligned in the radial and axial directions, respectively. Since $\hat{\boldsymbol{N}} \cdot \hat{\boldsymbol{n}}$ is nonzero on the inner surface, there is a net active force along $\hat{\mathbf{v}}$ that cannot be balanced by pressure gradients, provided the symmetry considerations guarantee that $\hat{\mathbf{v}} \cdot \nabla P = 0$. The same argument can be repeated for any two concentric cylinders inside the channel. We can thus conclude that spontaneous flow along $\hat{\mathbf{v}}$ must occur for arbitrarily small activity, as shown in Fig. 4(b).

We now proceed to compare the conclusion of the previous argument with an explicit solution of the approximate equations of motion in the frozen director limit. The analytic form for the ground-state director field in the one-Frank-constant approximation [see Fig. 4(a)] is given by

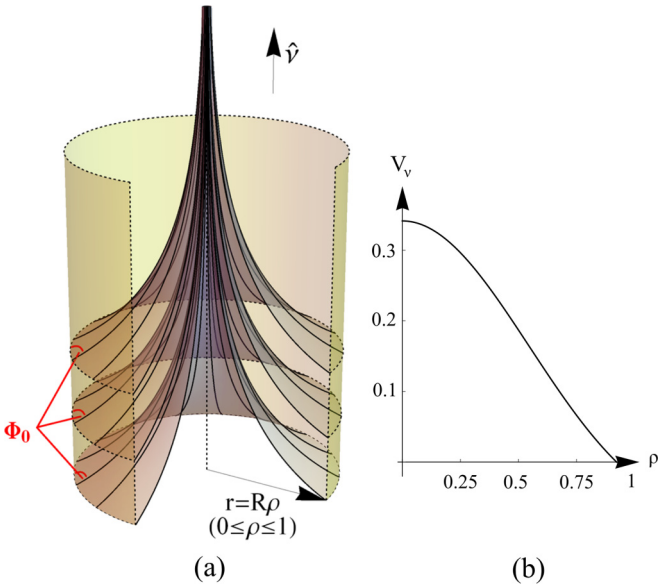

FIG. 4. Cylindrical bulk nematic with prescribed anchoring angle at the boundary. (a) Nematic director field lines with constant anchoring angle at the boundary Φ_0 (equal to 70° in the figure). (b) Plot of the magnitude of the velocity in the $\hat{\boldsymbol{\nu}}$ direction versus ρ, in the case of extensile activity ($\alpha < 0$). The velocity is measured in units of $2R|\alpha|/\eta$.

$\hat{\boldsymbol{n}} = \hat{\boldsymbol{\nu}}\cos\Phi - \hat{\boldsymbol{\rho}}\sin\Phi$, where $\rho \equiv r/R$ denotes the dimensionless radial coordinate and $\Phi(\rho)$ satisfies $\tan\frac{1}{2}\Phi(\rho) = \rho\tan\frac{1}{2}\Phi_0$ [50]. The corresponding active force reads

$$\boldsymbol{f}_a = \frac{4\alpha\gamma}{R(1+\gamma^2\rho^2)^3}[\hat{\boldsymbol{\rho}}(3-\gamma^2\rho^2)\gamma\rho - \hat{\boldsymbol{\nu}}(1-3\gamma^2\rho^2)], \tag{18}$$

where $\gamma \equiv \tan\frac{\Phi_0}{2}$. In order to solve for the flow $\boldsymbol{v}$ in $\nabla P - \eta\nabla^2\boldsymbol{v} = \boldsymbol{f}_a$, we use the fact that in a simply connected domain every vector field $\boldsymbol{f}_a$ has a unique (up to additive constants) Helmholtz decomposition $\boldsymbol{f}_a = \nabla\chi + \nabla\times\boldsymbol{A}$ with $\nabla\cdot\boldsymbol{A} = 0$, provided that on the boundary the normal component of $\nabla\times\boldsymbol{A}$ vanishes. Matching the terms respectively with ∇P and $\nabla^2\boldsymbol{v}$ gives

$$\nabla P = \frac{4\alpha\gamma^2\rho(3-\gamma^2\rho^2)}{R(1+\gamma^2\rho^2)^3}\hat{\boldsymbol{\rho}}, \quad \boldsymbol{\Omega}(\rho) = \frac{-2\alpha}{\eta}\frac{\gamma\rho(1-\gamma^2\rho^2)}{(1+\gamma^2\rho^2)^2}\hat{\boldsymbol{\theta}},$$

where the vorticity $\boldsymbol{\Omega}(\rho) \equiv \nabla\times\boldsymbol{v}$ and we have used the identity $\nabla^2\boldsymbol{v} = -\nabla\times\nabla\times\boldsymbol{v}$ (which holds since $\nabla\cdot\boldsymbol{v} = 0$). The relation

$$\iint_{\partial V} dS\,\hat{\boldsymbol{\tau}}\cdot\boldsymbol{\Omega} \approx -\frac{\alpha}{\eta}\int_{\partial V} dS(\hat{\boldsymbol{N}}\cdot\hat{\boldsymbol{n}}_0)(\hat{\boldsymbol{\nu}}\cdot\hat{\boldsymbol{n}}_0), \tag{19}$$

derived in Appendix D, fixes the constant of integration. Integrating again and taking into account the no-slip boundary condition for $\boldsymbol{v}$ then yields the solution

$$\boldsymbol{v} = \frac{-2R\alpha}{\gamma\eta}\left[\frac{1}{1+\gamma^2\rho^2} - \frac{1}{1+\gamma^2} + \frac{1}{2}\ln\frac{1+\gamma^2\rho^2}{1+\gamma^2}\right]\hat{\boldsymbol{\nu}}, \tag{20}$$

which is depicted in Fig. 4. The direction of flow is in the positive or negative $\hat{\boldsymbol{\nu}}$ direction depending on whether the active forces are extensile ($\alpha < 0$) or contractile ($\alpha > 0$). Note that the active force changes sign in the bulk if $\Phi_0 > \pi/3$, but this is not sufficient to reverse the flow. To see this, it can

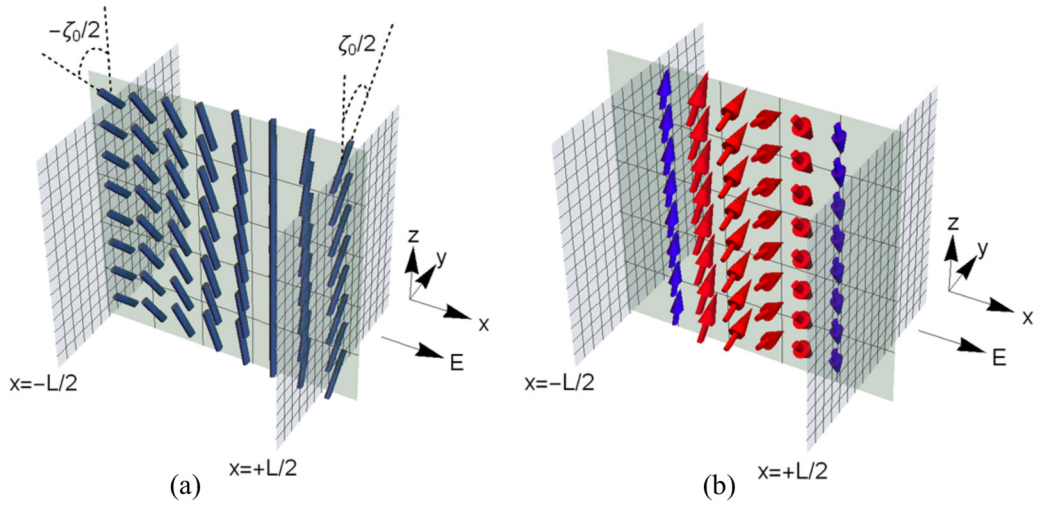

FIG. 5. (a) Director field ground state plotted in the plane $y = 0$. (b) Flow profile for the Frederiks cell illustrated by the velocity vector field plotted at $y = 0$. Note that there is net mass transport only in the y direction. A movie is available in the Supplemental Material [47].

be verified that

$$\frac{d\boldsymbol{v}}{d\rho} = \frac{2R\alpha\gamma\rho}{\eta} \cdot \frac{(1-\gamma^2\rho^2)}{(1+\gamma^2\rho^2)^2}\hat{\boldsymbol{v}}$$

and so, since $\gamma = \tan\Phi_0/2 \leqslant 1$ and $\rho \leqslant 1$, the only turning point in the bulk for $\boldsymbol{v}$ is at $\rho = 0$.

VII. ACTIVE PUMPS IN A FREDERIKS CELL

We now present the design of an active pump without moving parts based on a nematic Frederiks twist cell. Active liquid crystals controlled by a magnetic field have been recently realized experimentally [51], although in our case, the pump generates a persistent active flow that can be switched on by means of an applied electric field instead. As shown in Fig. 5(a), the setup for the cell is two parallel plates of infinite extent in the (y,z) plane at $x = \pm L/2$.

The plates are prepared with planar (parallel) anchoring but twisted relative to each other by an angle ζ_0. This pure twist nematic distortion leads to a vanishing active force, as noted earlier. However, if a sufficiently large electric field $\boldsymbol{E}$ is applied along the x direction, the familiar Frederiks instability [29] can be induced, in which the nematic director tilts towards the x direction inside the cell. This triggers a spontaneous transverse flow in the (y,z) plane, as can be deduced upon applying Eq. (17) (which is again exact using arguments similar to those used for the geometry of Fig. 3) to the volume enclosed by two planar boundaries parallel to the plates anywhere inside the cell. If the director is tilted on at least one of the two planar boundaries, then the right-hand side of Eq. (17) is different from zero and there is an active force along a direction of symmetry (i.e., the y direction) that cannot be balanced by pressure gradients (in fact, we will see later that $\nabla \cdot \boldsymbol{f}_a = 0$ and so $\nabla P = \mathbf{0}$ everywhere), resulting in flow.

In order to calculate the director field analytically, we parametrize it with the angles $\theta(x)$ and $\zeta(x)$, representing rotation about the y and x axes respectively, so that $\hat{\boldsymbol{n}} = \sin\theta(x)\hat{\boldsymbol{x}} + \cos\theta(x)[\sin\zeta(x)\hat{\boldsymbol{y}} + \cos\zeta(x)\hat{\boldsymbol{z}}]$, with $\theta(\pm L/2) = 0$ and $\zeta(\pm L/2) = \pm\zeta_0/2$. To provide a simplified illustration of the pump design, we assume a single Frank constant K. The resulting Euler-Lagrange equations read $K\nabla^2\hat{\boldsymbol{n}} + gn_x\hat{\boldsymbol{x}} = \mu(\boldsymbol{x})\hat{\boldsymbol{n}}$, where $\mu(\boldsymbol{x})$ is the Lagrange multiplier ensuring $\boldsymbol{n}^2 = 1$ and $g \equiv \epsilon_0\Delta\chi E^2$, where $\Delta\chi$ is the anisotropy in the electric susceptibility and ϵ_0 the permittivity of free space.

As detailed in Appendix H, the critical field (above which flow occurs) is given by $g_c = K(\pi/L)^2[1-(\zeta_0/\pi)^2]$, and writing $g = g_c + \Delta g$, the maximum tilt amplitude θ_0 is related to the incremental field Δg close to the transition by $\theta_0^2 = \frac{2\Delta g}{Kk^2(1-\gamma^2)}$, where we have defined $k \equiv \pi/L$ and $\gamma \equiv \zeta_0/\pi$. Working to $O(\theta_0)$, the solution for the director field [illustrated in Fig. 5(a)] is $\hat{\boldsymbol{n}} = \theta_0 \cos(kx)\hat{\boldsymbol{x}} + \hat{\boldsymbol{n}}_0$ where $\hat{\boldsymbol{n}}_0 \equiv \sin(\gamma kx)\hat{\boldsymbol{y}} + \cos(\gamma kx)\hat{\boldsymbol{z}}$. The corresponding active force reads

$$\boldsymbol{f}_a = -\alpha\theta_0 k[\sin(kx)\hat{\boldsymbol{n}}_0 + \gamma\cos(kx)\hat{\boldsymbol{x}} \times \hat{\boldsymbol{n}}_0], \tag{21}$$

leading to the flow [shown in Fig. 5(b)]

$$\begin{aligned} v_y &= \frac{\alpha\theta_0}{\eta k(1-\gamma^2)}\left[\sin\frac{\gamma\pi}{2} - \sin\gamma kx\sin kx - \gamma\cos\gamma kx\cos kx\right], \\ v_z &= \frac{\alpha\theta_0}{\eta k(1-\gamma^2)}\left[\frac{2}{\pi}kx\cos\frac{\gamma\pi}{2} - \cos\gamma kx\sin kx + \gamma\sin\gamma kx\cos kx\right], \end{aligned} \tag{22}$$

and $v_x = 0$. As previously noted, the flow occurs in the plane transverse to the electric field. Since either $\pm\theta_0$ may be selected, there is spontaneous symmetry breaking when the system selects the sign of θ_0 for the director field, which in turn determines the direction of the flow together with the sign of α. There is no net flow in the z direction as v_z is antisymmetric about $x = 0$. However, there is net flow in the y direction, with the maximum attained at $x = 0$.

VIII. CONCLUSION

In this article we have addressed what is perhaps the most well-known manifestation of active fluids: the onset of spontaneous active flow. Unlike polar active fluids composed of self-propelled particles, active nematics in a uniform configuration do not display net flow unless a critical threshold of activity (which is system size dependent) is exceeded. The mechanism of this instability has been extensively studied [2,18]. When activity overcomes the elastic energy it causes a continuous distortion of the alignment of the nematic molecules, which in turn generates an active force and hence flow. The typical experimental manifestation of this instability is a chaotic flow marked by the creation and annihilation of defect pairs in the nematic director.

In this work we have studied a different mechanism for spontaneous active flow in which flow is induced by special sets of nematic distortions that are imposed by means of curved substrates, boundaries, or external fields, without relying on activity itself to trigger such distortions. In this case, the only role of the active force is to balance frictional or drag forces at steady state (not to compete against elastic forces). As a result, the ensuing flow is laminar and occurs even for infinitesimally small values of the activity coefficient. Besides highlighting the relation between thresholdless active flow and symmetry breaking of the ground-state nematic director, our work may prove of practical interest in the developing field of active nematic microfluidics or experimental studies of living liquid crystals [13] under confinement.

Moreover, the ability to produce such controlled laminar active flows in active nematics makes it possible to study the mechanical response and excitations of materials that break time-reversal symmetry by organizing themselves in controlled nonequilibrium steady states. A recent example is the study of topological sound modes propagating within spontaneously flowing polar active liquids under confinement [19], which could now be generalized to active nematics. These topological sound modes can be viewed as electrons moving in a pseudo-magnetic-field induced by the background flow playing the role of a vector potential. Therefore, our strategies to induce active laminar flow (well below the instability threshold towards chaotic flow) represent a step towards engineering well-controlled persistent synthetic gauge fields in active nematics. Future work should clarify the topologically protected nature of the active nematic excitations that arise in the presence of such thresholdless laminar flows.

ACKNOWLEDGMENTS

We would like to thank Luca Giomi, Vinzenz Koning, Zvonomir Dogic, Alberto Fernandez Nieves, Jean-Francois Joanny, and Oleg Lavrentovich for helpful discussions. R.G. and V.V. acknowledge financial support from NWO via a VIDI grant and for V.V. this work was partially supported by the University of Chicago Materials Research Science and Engineering Center, which is funded by the National Science Foundation under award number DMR-1420709. J.T. thanks the Max Planck Institute for the Physics of Complex Systems (MPI-PKS), Dresden, Germany; the Kavli Institute for Theoretical Physics, Santa Barbara, CA; the DITP (NWO zwaartekracht) for financing his stay at the Instituut-Lorentz, Universiteit Leiden, and the Department of Bioengineering, Imperial College, London, UK for their hospitality while this work was under way. He also thanks the U.S. NSF for support through Grants No. EF-1137815 and No. 1006171 and the Simons Foundation for support through Grant No. 225579.

APPENDIX A: IRRELEVANCE OF NONEQUILIBRIUM MOLECULAR FIELDS

As noted in the main text, the equations of motion we have used are not, in fact, the most general. In particular, the Frank free energy F appearing in the Navier-Stokes equation (2a) need not, and indeed will not, be equal to that in the nematodynamic equation (2b), since we are dealing with a nonequilibrium system. Distinguishing these two free energies by writing them as F_v and F_n, we will now demonstrate that the fact that $F_v \neq F_n$ affects neither our criterion for flow nor, for small activity, the flow that occurs when this criterion is met.

Rewriting the equations of motion (2a)–(2c) taking into account this difference gives

$$\rho_0 \frac{Dv_k}{Dt} = -\partial_k P + \eta \nabla^2 v_k + \alpha \partial_j (n_j n_k) + \partial_j (\lambda_{ijk} h_{vi}), \tag{A1a}$$

$$\frac{Dn_i}{Dt} = \lambda_{ijk} \partial_j v_k - \frac{1}{\gamma_1} [h_{ni} - (h_{nj} n_j) n_i], \tag{A1b}$$

$$\nabla \cdot \boldsymbol{v} = 0, \tag{A1c}$$

where the molecular fields $\boldsymbol{h}_\nu$, $\nu = [v,n]$, appearing in these equations are given by $\boldsymbol{h}_\nu = \frac{\delta F_\nu}{\delta \hat{\boldsymbol{n}}}$, which implies

$$\boldsymbol{h}_\nu \equiv \frac{\delta F_\nu}{\delta \hat{\boldsymbol{n}}} = 2(K_{2\nu} - K_{3\nu})[\hat{\boldsymbol{n}} \cdot (\nabla \times \hat{\boldsymbol{n}})] \nabla \times \hat{\boldsymbol{n}} - K_{3\nu} \nabla^2 \hat{\boldsymbol{n}} + (K_{3\nu} - K_{2\nu}) \hat{\boldsymbol{n}} \times \nabla (\hat{\boldsymbol{n}} \cdot \nabla \times \hat{\boldsymbol{n}}) + (K_{3\nu} - K_{1\nu}) \nabla (\nabla \cdot \hat{\boldsymbol{n}}). \tag{A2}$$

Here the F_ν's, $\nu = [v,n]$, are the nonequilibrium generalizations of the equilibrium Frank free energy F. They are constrained by rotation invariance in exactly the same way as in equilibrium and must therefore both take the usual Frank free-energy [29] form

$$F_\nu = \frac{1}{2} \int d^3 r \{ K_{1\nu} (\nabla \cdot \hat{\boldsymbol{n}})^2 + K_{2\nu} [\hat{\boldsymbol{n}} \cdot (\nabla \times \hat{\boldsymbol{n}})]^2 + K_{3\nu} |\hat{\boldsymbol{n}} \times (\nabla \times \hat{\boldsymbol{n}})|^2 \}. \tag{A3}$$

However, although the form of the two free energies must be the same, away from equilibrium, the values of the Frank constants $K_{1,2,3}$ need not be the same in the two free energies. Only in equilibrium, in which the activity parameter $\alpha = 0$, do the two Frank free energies become equal ($F_v = F_n$). In an active system, however, the fundamentally nonequilibrium nature of the problem means that there are no such requirements of equality; that is, $F_v \neq F_n$ away from equilibrium, in contrast to the equations of motion (2a)–(2c), in which we took $F_v = F_n = F$. Our point here is that this is not, strictly speaking, true. Nonetheless, we do expect [18] that both α and the difference between F_v and F_n will be proportional to the density of active particles and will hence be very small when that density is small. Since we are interested in the small activity (i.e., low active particle density) limit, in the main text we ignored the difference between F_v and F_n. In this appendix

we show that none of the conclusions of the main text are altered by this difference. Specifically, we demonstrate first that for small activity, none of the flow fields $\boldsymbol{v}(\boldsymbol{r})$ that we calculated are quantitatively affected to leading order in activity α. Then we will show that our conclusions about the classes of configurations that do not exhibit thresholdless flow (e.g., pure twist) are completely unaffected by these differences to any order in α. This justifies our neglect of those differences in the main text.

We begin by considering situations in which the activity α does induce thresholdless flow. We will show that, even when α is very small, the terms involving $\boldsymbol{h}_v$ in Eq. (A1a) are always negligible, relative to the α terms. This is because, in the small activity limit, $\boldsymbol{h}_v \to \boldsymbol{h}_n$, with the difference $\boldsymbol{h}_v - \boldsymbol{h}_n \propto \alpha$, since, as noted earlier, the difference between $\boldsymbol{h}_v$ and $\boldsymbol{h}_n$ is a purely active effect. However, we have already shown in the main text that $\boldsymbol{h}_n \parallel \hat{\boldsymbol{n}}$; it is straightforward to show that when $\boldsymbol{h}_v \parallel \hat{\boldsymbol{n}}$, the terms involving $\boldsymbol{h}_v$ in Eq. (A1a) vanish. Hence, the only piece of those terms that can survive must arise from the difference $\boldsymbol{h}_v - \boldsymbol{h}_n$, which, as we have just argued, is proportional to α. However, these terms also involve more spatial derivatives of $\hat{\boldsymbol{n}}$ than the α term (to be precise, three versus one) and so on dimensional grounds, we expect the ratio of the $\boldsymbol{h}_v$ terms to the α terms to be $\sim(\frac{a}{L})^2$, where a is a microscopic length (e.g., the size of the active particles), while L is the length scale over which $\hat{\boldsymbol{n}}$ varies (usually a macroscopic length). Hence, the $\boldsymbol{h}_v$ terms in Eq. (A1a) are completely negligible, regardless of the value of α, in a macroscopic geometry. Note that the length a that appears in this estimate cannot be the instability length $L_{\text{inst}} \sim \sqrt{\frac{K}{\alpha}}$ discussed in the main text, since, as we just argued, the ratio of the $\boldsymbol{h}_v$ to the α term must be independent of α.

For the second case, in which there is no thresholdless flow, the nematic director must minimize the Frank free energy F_n. The Euler-Lagrange equations for the director field configurations $\hat{\boldsymbol{n}}_v(\boldsymbol{r})$ minimizing F_v are then simply

$$\boldsymbol{h}_v = \mu_v(\boldsymbol{r})\boldsymbol{n}_v, \tag{A4}$$

where $\mu_v(\boldsymbol{r})$ is a Lagrange multiplier. The active force $\boldsymbol{f}_a$ may be rewritten

$$\boldsymbol{f}_a = \alpha[\hat{\boldsymbol{n}}\nabla\cdot\hat{\boldsymbol{n}} - \hat{\boldsymbol{n}}\times(\nabla\times\hat{\boldsymbol{n}})]. \tag{A5}$$

Now let us consider the cases in which we argued in the main text that there could be no thresholdless flow. We will start with the case in which a pure twist configuration [i.e., one with $\nabla\cdot\hat{\boldsymbol{n}} = 0$ and $\hat{\boldsymbol{n}}\times(\nabla\times\hat{\boldsymbol{n}}) = \boldsymbol{0}$] minimizes F_n, the free energy appearing in the $\hat{\boldsymbol{n}}(\boldsymbol{r})$ equation of motion. We can immediately see that such a director field has no active force. One might wonder whether active flow in this case can be induced by the activity-induced difference between $\boldsymbol{h}_v$ and $\boldsymbol{h}_n$; we will now prove that this is not the case.

To see this, note that in a pure twist state, since $\hat{\boldsymbol{n}}\times(\nabla\times\hat{\boldsymbol{n}}) = \boldsymbol{0}$, $\nabla\times\hat{\boldsymbol{n}}$ must be parallel to $\hat{\boldsymbol{n}}$ itself. This implies that

$$\nabla\times\hat{\boldsymbol{n}} = g(\boldsymbol{r})\hat{\boldsymbol{n}}(\boldsymbol{r}), \tag{A6}$$

where $g(\boldsymbol{r})$ is some scalar function of $\boldsymbol{r}$. Furthermore, since $\hat{\boldsymbol{n}}$ is divergenceless in a pure twist state ($\nabla\cdot\hat{\boldsymbol{n}} = 0$), a well-known identity of vector calculus implies that $\nabla^2\hat{\boldsymbol{n}} = -\nabla\times(\nabla\times\hat{\boldsymbol{n}})$; using (A6) in this identity gives

$$\nabla^2\hat{\boldsymbol{n}} = -g\nabla\times\hat{\boldsymbol{n}} - \nabla g\times\hat{\boldsymbol{n}} = -g^2\hat{\boldsymbol{n}} + \hat{\boldsymbol{n}}\times\nabla g, \tag{A7}$$

where in the second equality we have used (A6) a second time. Using (A6), (A7), and $\nabla\cdot\hat{\boldsymbol{n}} = 0$ in our expression (A2) for the molecular field $\boldsymbol{h}_n$ gives

$$\boldsymbol{h}_n = (2K_{2n} - K_{3n})g^2\hat{\boldsymbol{n}} - K_{2n}\hat{\boldsymbol{n}}\times\nabla g. \tag{A8}$$

A moment's reflection reveals that, for this to be parallel to $\hat{\boldsymbol{n}}$, as it must be if we are to satisfy the director equation of motion (A1b) with $\boldsymbol{v} = \boldsymbol{0}$, we must have $\nabla g \parallel \hat{\boldsymbol{n}}$. For such a g, (A8) implies

$$\boldsymbol{h}_n = (2K_{2n} - K_{3n})g^2\hat{\boldsymbol{n}} \tag{A9}$$

and, by the same reasoning,

$$\boldsymbol{h}_v = (2K_{2v} - K_{3v})g^2\hat{\boldsymbol{n}}. \tag{A10}$$

Thus, for any pure twist configuration that gives $\boldsymbol{h}_n \propto \hat{\boldsymbol{n}}$ (which is just the condition for minimizing the Frank energy F_n subject to the constraint $|\hat{\boldsymbol{n}}| = 1$), the active force $\boldsymbol{f}_a$ vanishes and both $\boldsymbol{h}_v$ and $\boldsymbol{h}_n$ are everywhere parallel to $\hat{\boldsymbol{n}}$. However, the latter conditions imply, as noted earlier, that all of the terms involving $\boldsymbol{h}_v$ and $\boldsymbol{h}_n$ in Eqs. (A1a) and (A1b) vanish. Since $\boldsymbol{f}_a$ does as well, and all of the other terms in those equations vanish when $\boldsymbol{v} = \boldsymbol{0}$, we can conclude that, if $\hat{\boldsymbol{n}}$ is in a pure twist configuration that minimizes F_n, there will be no thresholdless active flow.

APPENDIX B: JUSTIFICATION OF THE FROZEN DIRECTOR AND ISOTROPIC VISCOSITY TENSOR APPROXIMATIONS AND APPLICATION IN THE CASE OF WEAK NEMATIC ORDER

We demonstrate here that the condition $\gamma_1 \ll \eta$ is sufficient to justify the frozen director approximation. We also show that any system with weak nematic order will be in this limit. We begin by noting that if the active and viscous terms are balanced in Eq. (2a), this implies schematically that if the system has a characteristic length scale L, then $\eta v/L^2 \sim \alpha/L$ and so $v \sim \alpha L/\eta$. This last result implies that the Reynolds number $\mathrm{Re} \equiv \frac{\rho_0 v L}{\eta} = \frac{\rho_0 L^2 \alpha}{\eta^2}$. Furthermore, using this estimate of v in Eq. (2b) and balancing the flow alignment terms $\lambda_{ijk}\partial_j v_k$ against the molecular field terms h_i, we obtain

$$\frac{1}{\gamma_1}\frac{\delta F}{\delta \hat{\boldsymbol{n}}} \sim \alpha/\eta. \tag{B1}$$

Note that the situation here is quite different from the usual case of flow alignment: In a classic flow alignment experiment, we apply a large shear flow to a large sample. In that case, the molecular fields h_i, which scale like $1/L^2$, cannot balance the flow alignment terms, which are proportional to the shear rate, which scales like $1/L$ for fixed boundary velocity. Hence, what happens instead is that the director field realigns itself by a large amount to make the $\lambda_{ijk}\partial_j v_k$ terms cancel each other. In our case, because the velocities induced by the active forces are, by assumption, small and the sample is small, the molecular fields can balance the flow alignment terms without substantial realignment of the director.

Assuming that α is small enough that $\mathrm{Re} \ll 1$, we can make the familiar Stokes approximation of neglecting the inertial terms on the left-hand side of Eq. (2a). Finally, we may neglect the λ term in Eq. (2a), which is of order $\frac{\gamma_1}{\eta}\frac{\alpha}{L}$ and is therefore smaller than the unperturbed active force by a factor of $\frac{\gamma_1}{\eta}$.

We also need to take into account the change in the active force resulting from the change in the director field $\delta\hat{\boldsymbol{n}} \equiv \hat{\boldsymbol{n}} - \hat{\boldsymbol{n}}_0$ induced by the flow; here $\hat{\boldsymbol{n}}_0$ is the equilibrium configuration of the nematic director (that is, the one that minimizes the Frank free energy or, equivalently, the field that is present before the activity is switched on). Since schematically the molecular field $\frac{\delta F}{\delta \hat{\boldsymbol{n}}} \sim \frac{K\delta n}{L^2}$ [note that δn appears in this expression rather than n because $(\frac{\delta F}{\delta \hat{\boldsymbol{n}}})_{\hat{\boldsymbol{n}}=\hat{\boldsymbol{n}}_0} = \boldsymbol{0}$], our estimate (B1) of that field implies that the magnitude δn of the perturbation in the director field must be of order $\frac{\alpha\gamma_1 L^2}{\eta K} \sim \frac{\gamma_1}{\eta}(\frac{L}{L_{\mathrm{inst}}})^2$, where L_{inst} is the length scale beyond which the uniform state becomes unstable. Since we are considering systems that are smaller than this length and since we are also assuming $\gamma_1 \ll \eta$, the change δn in $\hat{\boldsymbol{n}}$ is $\ll \hat{\boldsymbol{n}}_0$, the undistorted director configuration, and hence negligible.

To summarize, in the frozen director regime, defined as $\gamma_1 \ll \eta$, and small activity $\alpha \ll K/L^2$, we can determine the flow field simply by balancing the viscous force $\eta\nabla^2\boldsymbol{v}$ plus the pressure gradient $\boldsymbol{\nabla} P$ against the active force $\boldsymbol{f}_a$ computed for the unperturbed equilibrium configuration $\hat{\boldsymbol{n}}_0$ that minimizes the Frank free energy; that is, we can take the active force

$$\boldsymbol{f}_a = \alpha(\hat{\boldsymbol{n}} \cdot \boldsymbol{\nabla}\hat{\boldsymbol{n}} + \hat{\boldsymbol{n}}\boldsymbol{\nabla} \cdot \hat{\boldsymbol{n}}) \approx \alpha(\hat{\boldsymbol{n}}_0 \cdot \boldsymbol{\nabla}\hat{\boldsymbol{n}}_0 + \hat{\boldsymbol{n}}_0\boldsymbol{\nabla} \cdot \hat{\boldsymbol{n}}_0). \tag{B2}$$

Making this substitution and neglecting the λ term in Eq. (2a) simplifies (2a)–(2c) to

$$0 = -\nabla P + \eta\nabla^2 \boldsymbol{v} + \alpha(\hat{\boldsymbol{n}}_0 \cdot \nabla\hat{\boldsymbol{n}}_0 + \hat{\boldsymbol{n}}_0\nabla \cdot \hat{\boldsymbol{n}}_0) \tag{B3}$$

with $\nabla \cdot \boldsymbol{v} = 0$.

We now justify the isotropic viscosity approximation. In the limit of weak order, which in the notation of Kuzuu and Doi [32] is the limit $S_2, S_4 \ll 1$, our isotropic viscosity approximation becomes valid because α_4 (our activity parameter α should not be confused with Kuzuu and Doi's anisotropic viscosities), which is just the isotropic piece of the viscosity, is much greater than the anisotropic pieces $\alpha_{1,5,6}$ of the viscosity, since the latter all vanish when $S_{2,4} \to 0$, with (again in the notation of Kuzuu and Doi) $\eta = \alpha_4/2 \approx \eta^* C^3 r^2$. Furthermore, the coefficient $\gamma_1 = \alpha_3 - \alpha_2 = 10\eta^* C^3 r^2 S_2/\lambda$. Taking the ratio γ_1/η then gives $\gamma_1/\eta \approx 10S_2/\lambda$, which is always much less than 1 when the order is weak, since the flow alignment parameter λ is typically $O(1)$, and $S_2 \ll 1$ when the order is weak. We therefore expect our analytic solutions for the velocity fields, which assumed both isotropic viscosity and $\gamma_1 \ll \eta$ (to justify the frozen director approximation) to be quantitatively accurate in all active systems in which the nematic order is weak.

Note that no matter how strong the order is, at sufficiently long wavelengths, fluctuations in the nematic order parameter are much smaller than fluctuations in the nematic director. Hence, the director field representation is always a good approximation at sufficiently long wavelengths. In the case of weak nematic order, the nematic correlation length is of order a/S, where a is a molecular length ($\sim$1 nm) and S is the nematic order parameter. Taking $S \sim 0.01$, the nematic correlation length is of order 100 nm, much smaller than the size of a millimeter-sized sample.

We also note that this in particular implies that the frozen director approximation will always be valid for systems close to a weakly-first-order nematic to isotropic (N-I) transition. Since many N-I transitions are indeed weakly first order [29], this means it should be quite easy to experimentally test our quantitative predictions for the flow field.

Next, in the remainder of this section we extend the results of Sec. III in the case of a simply connected sample in the frozen director approximation, in which case the condition for thresholdless flow $\nabla \times \boldsymbol{f}_a \neq \boldsymbol{0}$ is necessary as well as sufficient. We consider the case in which the director field that minimizes F_n is pure splay, by which we mean $\nabla \times \hat{\boldsymbol{n}} = \boldsymbol{0}$. The curl of the active force is now given by

$$\nabla \times \boldsymbol{f}_a = \alpha\nabla \times [\hat{\boldsymbol{n}}\nabla \cdot \hat{\boldsymbol{n}}] = \alpha\nabla(\nabla \cdot \hat{\boldsymbol{n}}) \times \hat{\boldsymbol{n}}, \tag{B4}$$

which is also zero when the pure splay director field is a ground state of F_n, because the Euler-Lagrange equations that arise from minimizing F_n then require that $\boldsymbol{h}_n \parallel \hat{\boldsymbol{n}}$, which in turn, from (A2), requires that $\nabla(\nabla \cdot \hat{\boldsymbol{n}})$ is parallel to $\hat{\boldsymbol{n}}$. Furthermore, when $\nabla \times \hat{\boldsymbol{n}} = \boldsymbol{0}$, we can write $\hat{\boldsymbol{n}} = \nabla\Phi(\boldsymbol{r})$, which then implies $\boldsymbol{h}_v = -K_{1v}\nabla^2\nabla\Phi$, and $\boldsymbol{h}_n = -K_{1n}\nabla^2\nabla\Phi$. Thus, $\boldsymbol{h}_v \parallel \boldsymbol{h}_n$, so, if $\boldsymbol{h}_n \parallel \hat{\boldsymbol{n}}$ everywhere, $\boldsymbol{h}_v \parallel \hat{\boldsymbol{n}}$ everywhere as well. Hence, once again, the $\boldsymbol{h}_v$ and $\boldsymbol{h}_n$ terms in Eqs. (A1a) and (A1b), respectively, vanish, as does the curl of the active force. Under the conditions of this section we can conclude that there is no flow.

We now turn to the case of a pure bend field (i.e., one for which $\nabla \cdot \hat{\boldsymbol{n}} = \hat{\boldsymbol{n}} \cdot \nabla \times \hat{\boldsymbol{n}} = 0$). Using the identity $\nabla(\boldsymbol{A} \cdot \boldsymbol{B}) = (\boldsymbol{A} \cdot \nabla)\boldsymbol{B} + (\boldsymbol{B} \cdot \nabla)\boldsymbol{A} + \boldsymbol{A} \times (\nabla \times \boldsymbol{B}) + \boldsymbol{B} \times (\nabla \times \boldsymbol{A})$, with $\boldsymbol{A} = \hat{\boldsymbol{n}}$ and $\boldsymbol{B} = \nabla \times \hat{\boldsymbol{n}}$, and recalling that $\hat{\boldsymbol{n}} \cdot \nabla \times \hat{\boldsymbol{n}}$ must vanish in a pure bend field gives

$$(\hat{\boldsymbol{n}} \cdot \nabla)\nabla \times \hat{\boldsymbol{n}} + (\nabla \times \hat{\boldsymbol{n}} \cdot \nabla)\hat{\boldsymbol{n}} + \hat{\boldsymbol{n}} \times (\nabla \times \nabla \times \hat{\boldsymbol{n}}) = \boldsymbol{0}. \tag{B5}$$

If this pure bend state is also a ground state of F_n, the Euler-Lagrange equation (A4) for F_n is satisfied. For pure bend, that equation reduces to $\nabla^2\hat{\boldsymbol{n}} \parallel \hat{\boldsymbol{n}}$, so that $\hat{\boldsymbol{n}} \times (\nabla \times \nabla \times \hat{\boldsymbol{n}}) = -\hat{\boldsymbol{n}} \times \nabla^2\hat{\boldsymbol{n}} = \boldsymbol{0}$, thereby eliminating the last term of (B5). To compute $\nabla \times \boldsymbol{f}_a$, we now use the identity $\nabla \times (\boldsymbol{A} \times \boldsymbol{B}) = \boldsymbol{A}(\nabla \cdot \boldsymbol{B}) - \boldsymbol{B}(\nabla \cdot \boldsymbol{A}) + (\boldsymbol{B} \cdot \nabla)\boldsymbol{A} - (\boldsymbol{A} \cdot \nabla)\boldsymbol{B}$, again with $\boldsymbol{A} = \hat{\boldsymbol{n}}$ and $\boldsymbol{B} = \nabla \times \hat{\boldsymbol{n}}$, for $-\hat{\boldsymbol{n}} \times (\nabla \times \hat{\boldsymbol{n}})$, to get

$$\nabla \times \boldsymbol{f}_a = (\hat{\boldsymbol{n}} \cdot \nabla)\nabla \times \hat{\boldsymbol{n}} - (\nabla \times \hat{\boldsymbol{n}} \cdot \nabla)\hat{\boldsymbol{n}}. \tag{B6}$$

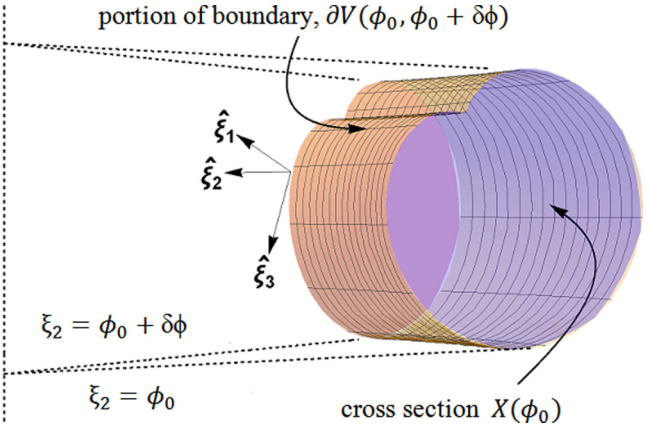

FIG. 6. Volume V' with cross section X bounded by the surfaces $\xi_2 = \phi_0$ and $\phi_0 + \delta\phi$. The faces of V' are $\partial V(\phi_0, \phi_0 + \delta\phi)$, $X(\phi_0)$, and $X(\phi_0 + \delta\phi)$.

Using our previous result (B5) together with $\hat{\boldsymbol{n}} \times (\boldsymbol{\nabla} \times \boldsymbol{\nabla} \times \hat{\boldsymbol{n}}) = \boldsymbol{0}$, we can rewrite this equation as

$$\boldsymbol{\nabla} \times \boldsymbol{f}_a = 2(\hat{\boldsymbol{n}} \cdot \boldsymbol{\nabla})\boldsymbol{\nabla} \times \hat{\boldsymbol{n}} = -2(\boldsymbol{\nabla} \times \hat{\boldsymbol{n}} \cdot \boldsymbol{\nabla})\hat{\boldsymbol{n}}. \tag{B7}$$

This is as far as we can go considering completely general pure bend configurations. To proceed further, we will now, in addition to imposing pure bend, add the additional restriction to 2D configurations, by which we mean that $\hat{\boldsymbol{n}}$ only depends on x and y, and has no z component, in some Cartesian coordinate system. Then $\boldsymbol{\nabla} \times \hat{\boldsymbol{n}}$ is in the z direction and so $(\boldsymbol{\nabla} \times \hat{\boldsymbol{n}} \cdot \boldsymbol{\nabla})\hat{\boldsymbol{n}} = \boldsymbol{0}$, which implies from (B7) that $\boldsymbol{\nabla} \times \boldsymbol{f}_a = \boldsymbol{0}$ as well. Similarly, we have that $\boldsymbol{h}_n = -K_{3n}\nabla^2\hat{\boldsymbol{n}} \parallel \hat{\boldsymbol{n}}$ by virtue of the Euler-Lagrange equations. Since $\boldsymbol{h}_v = -K_{3v}\nabla^2\hat{\boldsymbol{n}}$, this is also parallel to $\hat{\boldsymbol{n}}$ and so the $\boldsymbol{h}_v$ terms vanish, contributing nothing to Eq. (A1a).

We can thus conclude that under the conditions of this section, a two-dimensional active nematic with a director field in its ground state must have both splay and bend for there to be thresholdless flow in the absence of external fields. For fully three-dimensional configurations of an active nematic, on the other hand, for which there is also twist to take into account, it is unclear whether or not both splay and bend are necessary for thresholdless flow to occur in the absence of external fields. What we can conclude though is that, under the conditions of this section and in the absence of external fields, the ground-state director field must at the very least either have both splay and twist, or have bend, in order to induce thresholdless active flow.

In summary, we have identified three large classes of spatially nonuniform director configurations, namely, all pure twist and in the case of simply connected geometries in the frozen director approximation, all pure splay, and pure 2D bend, which do not induce thresholdless active flow. Thus, the requirements for thresholdless active flow are far more stringent than the mere existence of a spatially nonuniform director field.

APPENDIX C: DERIVATION OF GEOMETRIC INTEGRAL CONDITIONS FOR THRESHOLDLESS ACTIVE FLOW

Here we derive the geometric integral formula

$$\boldsymbol{F}(\phi_0) \cdot \hat{\boldsymbol{v}}(\phi_0) = \alpha \iint_{\partial V(\phi_0, \phi_0 + \delta\phi)} dS(\hat{\boldsymbol{N}} \cdot \hat{\boldsymbol{n}})(\hat{\boldsymbol{v}} \cdot \hat{\boldsymbol{n}}) + \alpha\delta\phi \iint_{X(\phi_0)} dS(\hat{\boldsymbol{v}} \times \hat{\boldsymbol{z}} \cdot \hat{\boldsymbol{n}})(\hat{\boldsymbol{v}} \cdot \hat{\boldsymbol{n}}) \tag{C1}$$

used in Sec. V for a sample with symmetry and arbitrary smooth cross section X, parametrized by general orthogonal curvilinear coordinates $\xi_{1,2,3}$ shown in Fig. 6. In the main text we make the

replacements in notation $\hat{\boldsymbol{\xi}}_1 \to \hat{\boldsymbol{N}}$, the normal to the bounding surface ∂V; $\hat{\boldsymbol{\xi}}_2 \to \hat{\boldsymbol{v}}$, the direction of symmetry; and $\hat{\boldsymbol{\xi}}_3 \to \hat{\boldsymbol{\tau}} = \hat{\boldsymbol{N}} \times \hat{\boldsymbol{v}}$. The net active force $\boldsymbol{F}(\phi_0)$ acting on this volume is given by

$$\boldsymbol{F}(\phi_0) = \iiint_{V'} h_1 h_2 h_3 d\xi_1 d\xi_2 d\xi_3 \boldsymbol{f}_a, \tag{C2}$$

where the geometrical scale factors $h_{1,2,3}$ are the ratios of the infinitesimal distances to infinitesimal changes $d\xi_{1,2,3}$ in the curvilinear coordinates (and should not, of course, be confused with the components of the molecular fields $\boldsymbol{h}$). Applying the divergence theorem to the component of $\boldsymbol{F}(\phi_0)$ along the direction $\hat{\boldsymbol{\xi}}_2$ enables us to convert the volume integral in Eq. (C2) into an integral over the surface $\partial V'$ of V':

$$\boldsymbol{F}(\phi_0) \cdot \hat{\boldsymbol{\xi}}_2(\phi_0) = \alpha \int_{\partial V'} dS (\hat{\boldsymbol{\xi}}_1 \cdot \hat{\boldsymbol{n}})(\hat{\boldsymbol{\xi}}_2 \cdot \hat{\boldsymbol{n}}). \tag{C3}$$

To evaluate this surface integral, we note that the surface $\partial V'$ of V' can be divided into three parts: the portion of the sample surface $\partial V(\phi_0, \phi_0 + \delta\phi)$ that borders V' and the two cross-sectional caps $X(\phi_0)$ and $X(\phi_0 + \delta\phi)$ (see Fig. 6). Doing so gives three surface integrals to evaluate, the first of which is

$$I^{\alpha}_{\partial V(\phi_0, \phi_0+\delta\phi)} = \alpha \hat{\boldsymbol{\xi}}_2(\phi_0) \cdot \int_{\phi_0}^{\phi_0+\delta\phi} d\xi_2 \int d\xi_3 h_2 h_3 n_1 n_i \hat{\boldsymbol{\xi}}_i.$$

Using the facts that the element of surface area $dS = d\xi_2 d\xi_3 h_2 h_3$, $n_1 = \hat{\boldsymbol{N}} \cdot \hat{\boldsymbol{n}}$, $\hat{\boldsymbol{n}} = n_i \hat{\boldsymbol{\xi}}_i$, and, in the notation of the main text, $\hat{\boldsymbol{\xi}}_2(\phi_0) = \hat{\boldsymbol{v}}$, we obtain the first term on the right-hand side of Eq. (C1):

$$I^{\alpha}_{\partial V(\phi_0, \phi_0+\delta\phi)} \approx \alpha \int_{\partial V(\phi_0, \phi_0+\delta\phi)} dS (\hat{\boldsymbol{N}} \cdot \hat{\boldsymbol{n}})(\hat{\boldsymbol{v}} \cdot \hat{\boldsymbol{n}}). \tag{C4}$$

Now evaluating the integrals across the cross sections, it is convenient to combine them as follows:

$$I^{\alpha}_{X(\phi_0)} = \alpha \hat{\boldsymbol{\xi}}_2(\phi_0) \cdot \int d\xi_1 d\xi_3 h_1 h_3 n_2 [-n_i \hat{\boldsymbol{\xi}}_i(\phi_0)],$$

$$I^{\alpha}_{X(\phi_0+\delta\phi)} = \alpha \hat{\boldsymbol{\xi}}_2(\phi_0) \cdot \int d\xi_1 d\xi_3 h_1 h_3 n_2 [n_i \hat{\boldsymbol{\xi}}_i(\phi_0 + \delta\phi)],$$

so that

$$I^{\alpha}_{X(\phi_0)} + I^{\alpha}_{X(\phi_0+\delta\phi)} \approx \alpha\delta\phi \hat{\boldsymbol{\xi}}_2 \cdot \int d\xi_1 d\xi_3 h_1 h_3 n_2 n_i \partial_2 \hat{\boldsymbol{\xi}}_i(\phi_0) \approx \alpha\delta\phi \int d\xi_1 d\xi_3 h_1 h_3 n_2 \hat{\boldsymbol{\xi}}_2 \cdot (n_i \partial_2 \hat{\boldsymbol{\xi}}_i), \tag{C5}$$

again taking $\hat{\boldsymbol{\xi}}_2$ inside the integral sign. The second term $I^{\alpha}_{X(\phi_0)} + I^{\alpha}_{X(\phi_0+\delta\phi)}$ can be simplified by noting that $\hat{\boldsymbol{\xi}}_2 \cdot \partial_2 \hat{\boldsymbol{\xi}}_i = \partial_2 \hat{\boldsymbol{\xi}}_2 \cdot \hat{\boldsymbol{\xi}}_i - \hat{\boldsymbol{\xi}}_i \cdot \partial_2 \hat{\boldsymbol{\xi}}_2$. Since $\hat{\boldsymbol{\xi}}_2 \cdot \hat{\boldsymbol{\xi}}_i = \delta_{i2}$, which is independent of ϕ, the first term vanishes. The argument of the integral in Eq. (C5) can then be rewritten $\hat{\boldsymbol{\xi}}_2 \cdot (n_i \partial_2 \hat{\boldsymbol{\xi}}_i) = -n_i \hat{\boldsymbol{\xi}}_i \cdot (\partial_2 \hat{\boldsymbol{\xi}}_2) = -\hat{\boldsymbol{n}} \cdot (\partial_2 \hat{\boldsymbol{\xi}}_2)$, where we have used the fact that $n_i \hat{\boldsymbol{\xi}}_i = \hat{\boldsymbol{n}}$ (this simply being the decomposition of $\hat{\boldsymbol{n}}$ along the local coordinate axes $\hat{\boldsymbol{\xi}}_i$). Now using the fact that $\partial_2 \hat{\boldsymbol{\xi}}_2 = \partial_\phi \hat{\boldsymbol{\phi}} = -\hat{\boldsymbol{r}}$, where $\hat{\boldsymbol{r}}$ is the unit vector in the radial direction from the axis of toroidal symmetry, we obtain

$$I^{\alpha}_{X(\phi_0)} + I^{\alpha}_{X(\phi_0+\delta\phi)} \approx \alpha\delta\phi \iint_{X(\phi_0)} dS [(\hat{\boldsymbol{v}} \times \hat{\boldsymbol{z}}) \cdot \hat{\boldsymbol{n}}](\hat{\boldsymbol{v}} \cdot \hat{\boldsymbol{n}}), \tag{C6}$$

where we have used the fact that $\hat{\boldsymbol{r}} = \hat{\boldsymbol{v}} \times \hat{\boldsymbol{z}}$. Adding this expression for the contribution of the cross sections $X(\phi_0)$ and $X(\phi_0 + \delta\phi)$ to the net toroidal force to that of the boundary ∂V as given by (C4) immediately gives Eq. (16).

High slenderness limit. In the case of torsional symmetry with an arbitrary (smooth) cross section X where the volume has a high slenderness σ, the second term in Eq. (16) may be dropped if the first term is nonzero. To see this, suppose that the length scale in the $\hat{\boldsymbol{\xi}}_1$ and $\hat{\boldsymbol{\xi}}_3$ directions is L, while in the $\hat{\boldsymbol{\xi}}_2$ direction it has a length scale of σL. A very slender sample will therefore have $\sigma \gg 1$, whereas a fat sample will have $\sigma \approx 1$. The first term in Eq. (16) is proportional to $L^2\sigma$, whereas the second term is proportional to L^2 and so can be neglected compared with the first term.

APPENDIX D: CONDITION ON THE VORTICITY FOR FLOW IN THE FROZEN DIRECTOR REGIME

Under the assumptions of Sec. V (i.e., torsional symmetry and that the pressure gradient is orthogonal to the direction of torsional symmetry $\hat{\boldsymbol{v}}$), we can provide a simple geometric statement of Eq. (B3) in terms of the vorticity of the flow $\boldsymbol{\Omega} \equiv \boldsymbol{\nabla} \times \boldsymbol{v}$ and the anchoring condition of the director at the boundary. If we apply the divergence theorem to Eq. (B3) over the pillbox volume V' in Fig. 1(a), we obtain

$$\eta \iint_{\partial V'} dS\, \hat{\boldsymbol{N}} \times \boldsymbol{\Omega} + \iint_{\partial V'} dS\, \hat{\boldsymbol{N}} P = \alpha \iint_{\partial V'} dS\, \hat{\boldsymbol{N}} \cdot \hat{\boldsymbol{n}}_0 \hat{\boldsymbol{n}}_0, \tag{D1}$$

using $\nabla^2 \boldsymbol{v} = -\boldsymbol{\nabla} \times \boldsymbol{\Omega}$ and the divergence theorem applied to $\boldsymbol{\nabla} \times \boldsymbol{\Omega}$. In the case of a slender sample, if we now again project along the direction of symmetry $\hat{\boldsymbol{v}}(\phi_0)$ and sum over all such pillbox volumes comprising the sample, we may take $\hat{\boldsymbol{v}}$ inside the integral and obtain

$$\iint_{\partial V} dS\, \hat{\boldsymbol{\tau}} \cdot \boldsymbol{\Omega} \approx -\frac{\alpha}{\eta} \int_{\partial V} dS (\hat{\boldsymbol{N}} \cdot \hat{\boldsymbol{n}}_0)(\hat{\boldsymbol{v}} \cdot \hat{\boldsymbol{n}}_0), \tag{D2}$$

where ∂V is now the boundary of the sample and $\hat{\boldsymbol{\tau}} = \hat{\boldsymbol{N}} \times \hat{\boldsymbol{v}}$.

APPENDIX E: ANALYSIS OF THE ACTIVE NEMATIC ON A TOROIDAL SHELL

Here we provide the calculation for the optimal value of ω in the ansatz

$$\hat{\boldsymbol{n}} = \frac{\omega\xi}{\xi + \cos\psi} \hat{\boldsymbol{\psi}} + \sqrt{1 - \left(\frac{\omega\xi}{\xi + \cos\psi}\right)^2}\, \hat{\boldsymbol{\phi}} \tag{E1}$$

for a toroidal nematic shell. The Frank free energy

$$\begin{aligned} F = \frac{1}{2} \int d^3\boldsymbol{r} \{ & K_1 (\boldsymbol{\nabla} \cdot \hat{\boldsymbol{n}})^2 + K_2 [\hat{\boldsymbol{n}} \cdot (\boldsymbol{\nabla} \times \hat{\boldsymbol{n}})]^2 + K_3 |\hat{\boldsymbol{n}} \times (\boldsymbol{\nabla} \times \hat{\boldsymbol{n}})|^2 \} \\ & - K_{24} \int d\boldsymbol{S} \cdot [\hat{\boldsymbol{n}} \boldsymbol{\nabla} \cdot \hat{\boldsymbol{n}} + \hat{\boldsymbol{n}} \times (\boldsymbol{\nabla} \times \hat{\boldsymbol{n}})] \equiv F_1 + F_2 + F_3 + F_{24} \end{aligned} \tag{E2}$$

must be minimized by varying the parameter ω. For completeness, we include the saddle-splay contribution to the Frank free energy (the K_{24} term), which can be relevant in curved geometries where the director field is not completely specified on the boundary, although we will show that there is no contribution in this case. For a thin shell, the ρ integral runs from $1 - \delta$ to 1, whereas the surface integral is taken over the surfaces $\rho = 1$ and $\rho = 1 - \delta$ where $\delta \ll 1$. In toroidal coordinates (ρ, ϕ, ψ), the scale factors are $(h_\rho, h_\phi, h_\psi) = R_2(1, \xi + \rho\cos\psi, \rho)$; for the ansatz (E1) it follows that

$$\boldsymbol{\nabla} \cdot \hat{\boldsymbol{n}} = \frac{\omega\xi^2 (1 - \rho)\sin\psi}{R_2 \rho (\xi + \rho\cos\psi)(\xi + \cos\psi)^2}, \tag{E3}$$

$$\boldsymbol{\nabla} \times \hat{\boldsymbol{n}} = \hat{\boldsymbol{\rho}} \frac{\sin\psi \left[\rho + \frac{\omega^2\xi^3(1-\rho)}{(\xi+\cos\psi)^3}\right]}{R_2 \rho (\xi + \rho\cos\psi)\sqrt{1 - \frac{\omega^2\xi^2}{(\xi+\cos\psi)^2}}} - \hat{\boldsymbol{\phi}} \frac{\omega\xi}{R_2 \rho (\xi + \rho\cos\psi)} + \hat{\boldsymbol{\psi}} \frac{\cos\psi \sqrt{1 - \frac{\omega^2\xi^2}{(\xi+\cos\psi)^2}}}{R_2 (\xi + \rho\cos\psi)}. \tag{E4}$$

As mentioned above, our first observation is that there is no contribution from saddle splay. To see this, note that for a shell of any thickness, F_{24} comprises two surface integrals, on the outside and the inside of the shell. Plugging the expressions (E4) and (E3) into (E2) over the outside surface only at $\rho = \rho_0$, we obtain

$$\frac{F_{24}^{\text{outside}}}{K_{24}} = -R_2 \int d\phi\, d\psi \left(\rho_0 \cos\psi + \frac{\omega^2 \xi^3}{(\xi + \cos\psi)^2} \right). \tag{E5}$$

As the first term is zero, only the second term remains and the integral is independent of ρ_0. Thus the integral over the inside surface exactly cancels that on the outside surface and $F_{24} = 0$.

For the volume integrals, since $\nabla \cdot \hat{\boldsymbol{n}} = 0$ at $\rho = 1$, we also have $F_1 = 0$. Since we expect that close to the transition ω will be small, we expand F_2 and F_3 to $O(\omega^4)$. The Frank free energy then takes the form $A\omega^4 + B\omega^2 + C + O(\omega^6)$, which has its minimum at $\omega^2 = -B/2A$, provided that $A > 0$ and $B < 0$. It is sufficient to expand the coefficient of ω^2 and ω^4 in $1/\xi$ to leading order; doing this gives

$$\frac{F_2}{K_2} = \frac{\delta}{2} \int d\phi\, d\psi \frac{\omega^2 \xi^4}{(\xi + \cos\psi)^4} \left(1 - \frac{\omega^2 \xi^2}{(\xi + \cos\psi)^2} \right) \approx \pi \delta \xi \int d\phi (\omega^2 - \omega^4), \tag{E6}$$

$$\frac{F_3}{K_3} = \frac{\delta}{2} \int d\phi\, d\psi \frac{\left(\cos\psi + \frac{\omega^2 \xi^3}{(\xi+\cos\psi)^2} \right)^2 + \frac{\sin^2\psi}{1 - \frac{\omega^2 \xi^2}{(\xi+\cos\psi)^2}}}{\xi + \cos\psi} \approx \pi \delta \xi \int d\phi \left(\text{const} - \omega^2 \frac{5}{2\xi^2} + \omega^4 \right). \tag{E7}$$

For chiral symmetry breaking, since we require that $A > 0$ and $B < 0$, we see that K_2/K_3 must be at least of order $1/\xi^2$. Thus, to leading order in $1/\xi$, we may neglect the higher-order terms in $1/\xi$ of each coefficient and the K_2 contribution to the ω^4 term, obtaining

$$\omega = \pm \sqrt{\frac{5}{4\xi^2} - \frac{K_2}{2K_3}}, \tag{E8}$$

provided that the expression under the square root is positive.

APPENDIX F: ANALYSIS OF A 3D BULK TOROIDAL NEMATIC

We now consider a 3D bulk version of the shell problem dealt with in Sec. IV B: a bulk toroid with planar anchoring and no slip on the surface. For very slender tori (which are nearly cylinders) the nematic director will be everywhere oriented along $\hat{\boldsymbol{v}} = \hat{\boldsymbol{\phi}}$, the direction of torsional symmetry. Recent experimental and theoretical studies [42,43] have shown that as the aspect ratio of the tori is lowered (i.e., as we move towards fatter tori), a structural transition to a chiral configuration takes place in the ground state, leading to the twisted nematic texture shown in Fig. 7.

The following double-twist ansatz has proved effective in capturing the qualitative features of the chiral symmetry-breaking transition in the ground state at zero activity [42–44]:

$$\hat{\boldsymbol{n}} = \frac{\omega \xi \rho}{\xi + \rho \cos\psi} \hat{\boldsymbol{\psi}} + \sqrt{1 - \left(\frac{\omega \xi \rho}{\xi + \rho \cos\psi} \right)^2} \hat{\boldsymbol{\phi}}, \tag{F1}$$

where ω is a variational parameter describing the degree of twist in the director field. In this expression, (ρ, ϕ, ψ) are toroidal coordinates [see Fig. 8(a)], where ρ is the dimensionless radial coordinate varying between 0 and 1, ψ is the poloidal angle, ϕ is the toroidal or azimuthal angle, and the slenderness of the torus $\xi \equiv R_1/R_2$ is the aspect ratio of its major (R_1) and minor (R_2) radii.

To leading order in $1/\xi$, the ground states shown in Figs. 7(a) and 7(c) are $\omega = \pm 2\sqrt{\frac{5}{16\xi^2} - \frac{K_2 - K_{24}}{K_3}}$, provided that the quantity under the square root is positive (otherwise the ground state is the untwisted

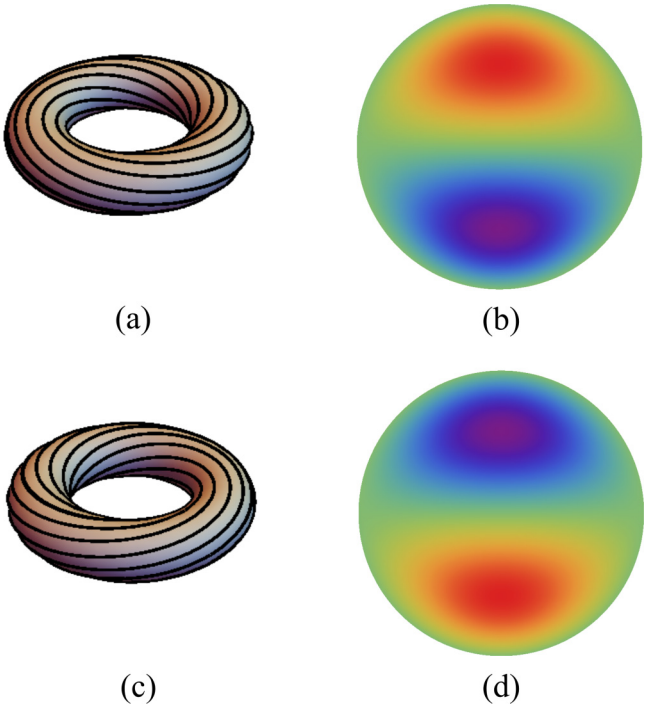

FIG. 7. (a) Nematic director field lines of an active nematic in the left chiral ground state ($\omega < 0$) and associated flow in cross section (b). (c) Nematic director field lines of an active nematic in the right chiral ground state ($\omega > 0$) and associated flow in cross section (d). Activity is extensile ($\alpha < 0$); red denotes flow in the negative ϕ direction, violet denotes flow in the positive ϕ direction, and green denotes no flow. See Supplemental Material [47] for a movie of this flow.

state $\omega = 0$). To $O(\omega)$, the active force reads

$$\boldsymbol{f}_a = \frac{-\alpha\left(\hat{\boldsymbol{\rho}}\cos\psi - \hat{\boldsymbol{\psi}}\sin\psi + \hat{\boldsymbol{\phi}}\frac{\omega\xi\rho\sin\psi}{\xi+\rho\cos\psi}\right)}{R_2(\xi+\rho\cos\psi)}. \tag{F2}$$

In Appendix B we showed that in the frozen director regime Eqs. (2a)–(2c) reduce to

$$0 = -\nabla P + \eta\nabla^2\boldsymbol{v} + \alpha(\hat{\boldsymbol{n}}_0\cdot\nabla\hat{\boldsymbol{n}}_0 + \hat{\boldsymbol{n}}_0\nabla\cdot\hat{\boldsymbol{n}}_0) \tag{F3}$$

with $\nabla\cdot\boldsymbol{v} = 0$. Using this and taking the divergence of Eq. (F3) implies that $\nabla^2 P = 0$. If the pressure is independent of the azimuthal coordinate ϕ, to $O(\omega)$, the solution for the pressure

$$P = -\alpha\ln(\xi+\rho\cos\psi) \tag{F4}$$

cancels the source term's ρ and ψ components. If we now write $\boldsymbol{v} = \boldsymbol{u}(\rho,\psi) + v_\phi(\rho,\psi)\hat{\boldsymbol{\phi}}$, where $\boldsymbol{u}(\rho,\psi)$ is the projection of $\boldsymbol{v}$ on the (ρ,ψ) plane, $\boldsymbol{u}$ vanishes on the boundary and so throughout the bulk. Thus (F3) reduces to

$$\nabla^2(v_\phi\hat{\boldsymbol{\phi}}) = \frac{\alpha\omega\xi\rho\sin\psi}{\eta R_2(\xi+\rho\cos\psi)}\hat{\boldsymbol{\phi}}, \tag{F5}$$

with $v_\phi = 0$ at $\rho = 1$. As

$$\nabla^2(v_\phi(r,\psi)\hat{\boldsymbol{\phi}}) = \hat{\boldsymbol{\phi}}\left(\nabla^2 - \frac{1}{R_2^2(\xi+\rho\cos\psi)^2}\right)v_\phi = \hat{\boldsymbol{\phi}}\frac{1}{\cos\phi}\nabla^2(v_\phi\cos\phi), \tag{F6}$$

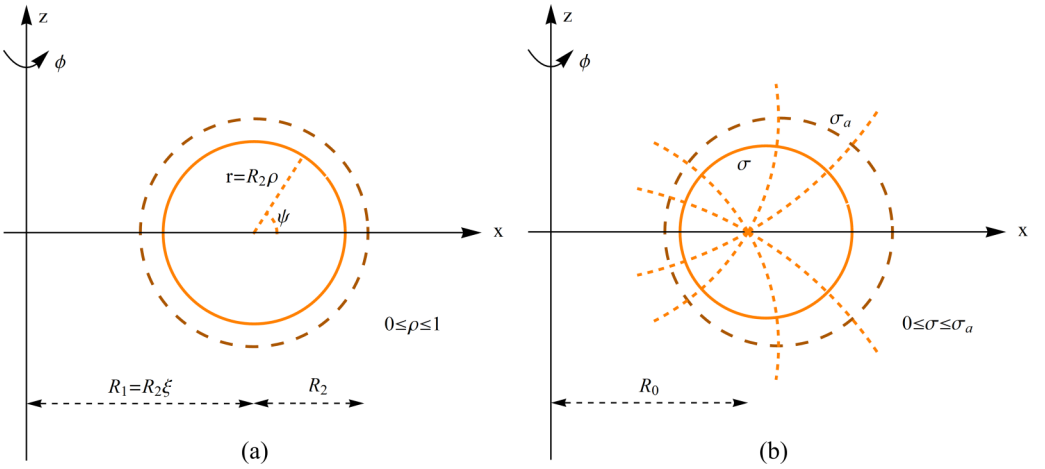

FIG. 8. Two coordinate systems used to parametrize a toroid. The plane $y = 0$ is shown for the $x \geqslant 0$ half of the toroid using (a) (ρ,ϕ,ψ) coordinates, where ψ is the poloidal angle and ϕ the azimuthal angle, and (b) (σ,τ,ϕ) coordinates in which $\sigma \in [0,\sigma_a]$ with $\sigma_a < 1$. Curves of constant τ are shown, increasing from 0 to 2π in the clockwise direction and converging at the point $(x = R_0, z = 0)$.

it is sufficient to solve

$$\nabla^2[v_\phi(r,\psi)\cos\phi] = \frac{\alpha\omega\xi\rho\sin\psi\cos\phi}{\eta R_2(\xi+\rho\cos\psi)^2}. \tag{F7}$$

In order to do this, we make use of the Green's function for the scalar Poisson equation with vanishing boundary conditions on the surface of a toroid. This is specified in alternative toroidal coordinates (σ,τ,ϕ), which are shown in Fig. 8(b). Mapping our (ρ,ϕ,ψ) coordinates to (σ,τ,ϕ), first we note that

$$\begin{aligned}
\boldsymbol{x} &= R_2[(\xi+\rho\cos\psi)\cos\phi,(\xi+\rho\cos\psi)\sin\phi,\rho\sin\psi],\\
\hat{\boldsymbol{\rho}} &= [\cos\psi\cos\phi,\cos\psi\sin\phi,\sin\psi],\\
\hat{\boldsymbol{\psi}} &= [-\sin\psi\cos\phi,-\sin\psi\sin\phi,\cos\psi],\\
\hat{\boldsymbol{\phi}} &= [-\sin\phi,\cos\phi,0],
\end{aligned} \tag{F8}$$

where $[A_x,A_y,A_z] \equiv A_x\hat{\boldsymbol{x}} + A_y\hat{\boldsymbol{y}} + A_z\hat{\boldsymbol{z}}$ is shorthand for Cartesian coordinates. The scaling factors in our original coordinate system are

$$h_\rho = R_2, \quad h_\phi = R_2(\xi+\rho\cos\psi), \quad h_\psi = R_2\rho. \tag{F9}$$

In the alternative coordinate system,

$$\begin{aligned}
\boldsymbol{x} &= \frac{R_0}{1-\sigma\cos\tau}[\sqrt{1-\sigma^2}\cos\phi,\sqrt{1-\sigma^2}\sin\phi,-\sigma\sin\tau]\\
&= R_0(1+\sigma\cos\tau)\left[\cos\phi,\sin\phi,\frac{-\sigma\sin\tau}{(1+\sigma\cos\tau)}\right] + O(\sigma^2),\\
\hat{\boldsymbol{\sigma}} &= [\cos\tau\cos\phi,\cos\tau\sin\phi,-\sin\tau] + O(\sigma),\\
\hat{\boldsymbol{\tau}} &= [-\sin\tau\cos\phi,-\sin\tau\sin\phi,-\cos\tau] + O(\sigma),\\
\hat{\boldsymbol{\phi}} &= [-\sin\phi,\cos\phi,0].
\end{aligned} \tag{F10}$$

The surface $\sigma = \text{const}$ ($0 \leqslant \sigma < 1$) describes the surface of a torus with major radius $R_1 = R_0/\sqrt{1-\sigma^2}$ and minor radius $r = R_0\sigma/\sqrt{1-\sigma^2}$, as can be seen from the fact that x, y, and z above satisfy

$$\left(\sqrt{x^2+y^2} - \frac{R_0}{\sqrt{1-\sigma^2}}\right)^2 + z^2 = \frac{R_0^2\sigma^2}{1-\sigma^2}. \tag{F11}$$

The scaling factors in the new coordinate system are

$$h_\sigma = \frac{R_0}{\sqrt{1-\sigma^2}(1-\sigma\cos\tau)}, \quad h_\tau = \frac{R_0\sigma}{1-\sigma\cos\tau}, \quad h_\phi = \frac{R_0\sqrt{1-\sigma^2}}{1-\sigma\cos\tau}. \tag{F12}$$

Translating between the original and alternative toroidal coordinate systems,

$$\begin{aligned} R_2 = \frac{R_0\sigma_a}{\sqrt{1-\sigma_a^2}}, \quad \rho = \sqrt{\frac{1-\sigma_a^2}{1-\sigma^2}}\frac{\sigma}{\sigma_a}, \quad \xi = \frac{R_1}{R_2} = \frac{1}{\sigma_a} \\ R_2(\xi + \rho\cos\psi) = \frac{R_0\sqrt{1-\sigma^2}}{1-\sigma\cos\tau}, \quad \frac{\rho\sin\psi}{\xi+\rho\cos\psi} = \frac{-\sigma\sin\tau}{\sqrt{1-\sigma^2}} \end{aligned} \tag{F13}$$

and Eq. (F7) may be expressed in (σ,τ,ϕ) coordinates to $O(\sigma_a)$ as

$$\nabla^2[v_\phi(\sigma,\tau)\cos\phi] = \frac{-\alpha\omega\sigma\sin\tau\cos\phi}{\eta R_2} + O\left(\sigma_a^2\right). \tag{F14}$$

In this coordinate system, we may now use the Green's function for the Laplacian vanishing on the surface of a toroid with $\sigma = \sigma_a$, which is given by [52]

$$\begin{aligned} G(\boldsymbol{x},\boldsymbol{x}') = {} & \frac{1}{\pi R_0}\sqrt{1-\sigma\cos\tau}\sqrt{1-\sigma'\cos\tau'}\sum_{n=0}^{\infty}\sum_{m=0}^{\infty}(-1)^n\epsilon_n\epsilon_m\frac{\Gamma(m-n+1/2)}{\Gamma(m+n+1/2)}g_{mn} \\ & \times \cos m(\tau-\tau')\cos n(\phi-\phi'), \end{aligned} \tag{F15}$$

where $g_{mn} \equiv g_{mn}(\sigma',\sigma,\sigma_a)$ is given by

$$g_{mn} \equiv \frac{T_{mn}(\sigma_<)}{T_{mn}(\sigma_a)}[T_{mn}(\sigma_a)S_{mn}(\sigma_>) - T_{mn}(\sigma_>)S_{mn}(\sigma_a)],$$

ϵ_n is 1 if $n = 0$ and 2 otherwise, and $\sigma_>$ and $\sigma_<$ denote the higher and lower of σ and σ', respectively. In addition, $T_{mn}(\sigma)$ and $S_{mn}(\sigma)$ are toroidal harmonic functions defined as

$$T_{mn}(\sigma) \equiv \sigma^{-1/2}Q^n_{m-1/2}(1/\sigma), \quad S_{mn}(\sigma) \equiv \sigma^{-1/2}P^n_{m-1/2}(1/\sigma), \tag{F16}$$

where the functions $Q^\lambda_\nu(1/\sigma)$ and $P^\lambda_\nu(1/\sigma)$ are the associated Legendre functions of order λ and degree ν. Applying the Green's function to the source and using the asymptotic forms [53] $T_{11}(\sigma) \sim -\frac{3\pi}{8\sqrt{2}}\sigma$ and $S_{11}(\sigma) \sim \frac{\sqrt{2}}{\pi}\sigma^{-1}$ for $\sigma \ll 1$ gives, to leading order in $\sigma_a = 1/\xi$,

$$\begin{aligned} v_\phi &= -\frac{4\alpha\omega R_2\sigma_a}{3\eta}\sin\tau\frac{1}{\sigma_a^3}\int_0^{\sigma_a} d\sigma'\sigma'^2 g_{11} + O\left(\sigma_a^2\right) \\ &= \frac{\alpha\omega R_2\sigma_a}{8\eta}\sin\tau s(1-s^2) + O\left(\sigma_a^2\right) = -\frac{\alpha\omega R_2}{8\eta\xi}\sin\psi\rho(1-\rho^2) + O(1/\xi^2), \end{aligned} \tag{F17}$$

where $s \equiv \sigma/\sigma_a$ and we have used the results (F13) to translate back to (ρ,ϕ,ψ) coordinates.

Thus, when there is a chiral twisted ground state, the activity creates a flow one way in the $\hat{\boldsymbol{\phi}}$ direction in the top half of the toroid and in the opposite direction in the bottom half. The orientation of the flow is determined by the sign of the activity (contractile or extensile) and the chirality of the ground state, as illustrated in Fig. 7.

APPENDIX G: PARALLEL PLATES WITH MIXED BOUNDARY CONDITIONS

We consider a two-dimensional system confined between two infinite plates, which has been previously studied numerically [25]. The configuration is shown in Fig. 3(a); the plates are orthogonal to the x axis, separated by a distance L, and prepared with homeotropic alignment (in the x direction) on one plate and planar alignment (in the y direction) on the other.

We will begin by demonstrating that for any values of the Frank constants, this geometry leads to thresholdless flow. Seeking a solution of the form

$$\hat{\boldsymbol{n}} = \hat{\boldsymbol{x}}\cos\theta(x) + \hat{\boldsymbol{y}}\sin\theta(x) \tag{G1}$$

to the Euler-Lagrange equations for (4),

$$\begin{aligned}\mu(\boldsymbol{r})\hat{\boldsymbol{n}} = \boldsymbol{h} \equiv \frac{\delta F}{\delta \hat{\boldsymbol{n}}} &= 2(K_2 - K_3)[\hat{\boldsymbol{n}}\cdot(\nabla\times\hat{\boldsymbol{n}})]\nabla\times\hat{\boldsymbol{n}} - K_3\nabla^2\hat{\boldsymbol{n}} + (K_3 - K_2)\hat{\boldsymbol{n}}\times\nabla(\hat{\boldsymbol{n}}\cdot\nabla\times\hat{\boldsymbol{n}}) \\ &\quad + (K_3 - K_1)\nabla(\nabla\cdot\hat{\boldsymbol{n}}),\end{aligned} \tag{G2}$$

where $\mu(\boldsymbol{r})$ is a Lagrange multiplier, leads to $\nabla\times\boldsymbol{n} = \hat{\boldsymbol{z}}\theta'\cos(\theta)$. Taking this together with (G1) implies that the twist vanishes ($\boldsymbol{n}\cdot\nabla\times\boldsymbol{n} = 0$). Using this and (G1) in the Euler-Lagrange equation (G2) leads to

$$K_1(\theta'^2\cos\theta + \theta''\sin\theta)\hat{\boldsymbol{x}} + K_3(\theta'^2\sin\theta - \theta''\cos\theta)\hat{\boldsymbol{y}} = \mu(\boldsymbol{r})[\hat{\boldsymbol{x}}\cos\theta(x) + \hat{\boldsymbol{y}}\sin\theta(x)]. \tag{G3}$$

From the y component of Eq. (G3) it follows that

$$\mu(\boldsymbol{r})\sin\theta = K_3(\theta'^2\sin\theta - \theta''\cos\theta). \tag{G4}$$

Using this relation in the x component of (G3) gives

$$K_1(\theta'^2\cos\theta + \theta''\sin\theta)\tan\theta = K_3(\theta'^2\sin\theta - \theta''\cos\theta), \tag{G5}$$

which can be solved for θ'':

$$\theta'' = \frac{(K_3 - K_1)\theta'^2\sin(2\theta)}{2(K_1\sin^2\theta + K_3\cos^2\theta)}. \tag{G6}$$

From this solution, it is straightforward to show that

$$\theta' = \frac{k}{\sqrt{1 + \left(\frac{K_3 - K_1}{K_3 + K_1}\right)\cos(2\theta)}}, \tag{G7}$$

where the constant of integration $k \neq 0$, since the boundary conditions do not allow $\theta(x)$ to be a constant. Hence, (G7) implies that $\theta' \neq 0$ throughout the sample. Using the original ansatz (G1) to calculate the curl of the active force gives, after some algebra,

$$\nabla\times\boldsymbol{f}_a = \alpha\hat{\boldsymbol{z}}[\theta''\cos(2\theta) - 2\theta'^2\sin(2\theta)]. \tag{G8}$$

Using our solution (G6) for θ'' in Eq. (G8) gives

$$\nabla\times\boldsymbol{f}_a = \alpha\theta'^2\sin(2\theta)\hat{\boldsymbol{z}}\left[\frac{(K_3 - K_1)\cos(2\theta)}{2(K_1\sin^2\theta + K_3\cos^2\theta)} - 2\right]. \tag{G9}$$

Since, as we showed earlier, $\theta' \neq 0$ throughout the sample and the expression in the square brackets is strictly negative, (G9) implies that $\nabla\times\boldsymbol{f}_a \neq \boldsymbol{0}$ throughout the sample, except at the points where θ is an integer multiple of $\pi/2$. Since $\nabla\times\boldsymbol{f}_a \neq \boldsymbol{0}$, there must be flow, as noted in the main text.

From (G7), we see that the case $K_1 = K_3$ (as in the commonly made one-Frank-constant approximation previously studied numerically [25]) is particularly simple, since $\theta' = k$, which implies $\theta = kx + C$, where C is another constant of integration. The constants C and k can be easily determined from the boundary conditions $\theta(x = 0) = 0$ and $\theta(x = L) = \frac{\pi}{2}$, which imply $k = \pi/2L$ and $C = 0$. Thus the director field ground state has the solution

$$\hat{\boldsymbol{n}} = \hat{\boldsymbol{x}}\cos kx + \hat{\boldsymbol{y}}\sin kx, \tag{G10}$$

which leads to the active force density

$$\boldsymbol{f}_a = \alpha(\boldsymbol{n}\nabla\cdot\boldsymbol{n} - \boldsymbol{n}\times\nabla\times\boldsymbol{n}) = \alpha k(-\hat{\boldsymbol{x}}\sin 2kx + \hat{\boldsymbol{y}}\cos 2kx). \tag{G11}$$

To actually determine this flow $\boldsymbol{v}(\boldsymbol{r})$, we use the unique Helmholtz decomposition into parts with pure gradient and pure curl. Matching these terms respectively with ∇P and $\nabla^2\boldsymbol{v}$, as in Eq. (B3), and taking into account the no-slip boundary conditions yields

$$P = \frac{\alpha}{2}\cos 2kx, \quad \boldsymbol{v} = \frac{\alpha L}{2\pi\eta}\left(\cos\frac{\pi x}{L} + 2\frac{x}{L} - 1\right)\hat{\boldsymbol{y}}. \tag{G12}$$

As can be seen in Fig. 3(b), the flow profile is antisymmetric about the midpoint between the plates at $x = L/2$. Thus there is no net mass transport in this simple example. Net mass transport is possible, however, if the alignment angle on the boundary is modified; for example, if it were possible for the right-hand plate to be prepared so that the director field made an angle of $\pi/4$ with the normal, then just the left-hand half of Fig. 3 would be realized, with flow now only in the positive y direction.

Net mass transport also occurs if $K_1 \neq K_3$. Consider the extreme case when $K_1 \gg K_3$; then (G7) implies $\theta' = \frac{k}{\sqrt{2}\sin\theta}$, which in turn implies

$$\cos\theta = C - \frac{k}{\sqrt{2}}x, \tag{G13}$$

where C is another constant of integration. The boundary conditions $\theta(x=0) = 0$ and $\theta(x = L) = \frac{\pi}{2}$ now imply $k = \frac{\sqrt{2}}{L}$ and $C = 1$. Using these in Eq. (G13) then gives

$$\begin{aligned}\hat{\boldsymbol{n}} &= \hat{\boldsymbol{x}}\left(1 - \frac{x}{L}\right) + \hat{\boldsymbol{y}}\sqrt{2\frac{x}{L} - \left(\frac{x}{L}\right)^2},\\ \boldsymbol{f}_a &= -\frac{2\alpha}{L}\left(1 - \frac{x}{L}\right)\hat{\boldsymbol{x}} + \alpha\partial_x\left[\left(1 - \frac{x}{L}\right)\sqrt{2\frac{x}{L} - \left(\frac{x}{L}\right)^2}\right]\hat{\boldsymbol{y}}.\end{aligned} \tag{G14}$$

The solutions for the pressure P and velocity field $\boldsymbol{v}$ are now

$$P = -\alpha\left[2\frac{x}{L} - \left(\frac{x}{L}\right)^2\right], \quad \boldsymbol{v} = \hat{\boldsymbol{y}}\frac{\alpha L}{3\eta}\left\{\frac{x}{L} - \left[2\frac{x}{L} - \left(\frac{x}{L}\right)^2\right]^{3/2}\right\}, \tag{G15}$$

for which there is a net mass transport J in the y direction per unit length in the z direction given by

$$J = \left(\frac{8 - 3\pi}{48}\right)\frac{\rho_0\alpha L^2}{\eta}. \tag{G16}$$

The velocity field (G15) is illustrated in Fig. 3(d), which shows that nearly all of the flow is in the positive y direction.

APPENDIX H: ANALYSIS OF THE FREDERIKS CELL ACTIVE PUMP

Our starting point is the following parametrization for the director field [see Fig. 5(a)]:

$$\hat{\boldsymbol{n}} = \sin\theta(x)\hat{\boldsymbol{x}} + \cos\theta(x)\hat{\boldsymbol{t}}(x), \tag{H1}$$

where we have defined an x-dependent unit vector orthogonal to $\hat{\boldsymbol{x}}$:

$$\hat{\boldsymbol{t}}(x) \equiv \sin\zeta(x)\hat{\boldsymbol{y}} + \cos\zeta(x)\hat{\boldsymbol{z}}. \tag{H2}$$

The boundary conditions, expressed in terms of the angles $\theta(x)$ and $\zeta(x)$, are $\theta(\pm L/2) = 0$ and $\zeta(\pm L/2) = \pm\zeta_0/2$. Making the single-Frank-constant approximation ($K_{1,2,3} \equiv K$), the Euler-

Lagrange equation for $\hat{\boldsymbol{n}}$ is

$$K\frac{d^2\hat{\boldsymbol{n}}(x)}{dx^2} + gn_x(x)\hat{\boldsymbol{x}} = \mu(x)\hat{\boldsymbol{n}}, \tag{H3}$$

where $\mu(\boldsymbol{x})$ is the Lagrange multiplier ensuring that $\boldsymbol{n}^2 = 1$ and $g \equiv \epsilon_0 \Delta\chi E^2$ can be experimentally controlled with an electric field E.

Since $\hat{\boldsymbol{t}}(x)$ is a unit vector in the plane orthogonal to $\hat{\boldsymbol{x}}$, its derivative must be a vector orthogonal to itself in that plane, whose magnitude is $\zeta'(x) \equiv \frac{d\zeta}{dx}$. This observation implies

$$\frac{d\hat{\boldsymbol{t}}(x)}{dx} = \zeta'(x)\hat{\boldsymbol{t}} \times \hat{\boldsymbol{x}}, \tag{H4}$$

repeated application of which in turn leads to a natural decomposition of $\frac{d^2\hat{\boldsymbol{n}}(x)}{dx^2}$ along the orthonormal triad $\hat{\boldsymbol{t}}$, $\hat{\boldsymbol{x}}$, and $\hat{\boldsymbol{t}} \times \hat{\boldsymbol{x}}$:

$$\begin{aligned}\frac{d^2\hat{\boldsymbol{n}}(x)}{dx^2} &= [\theta'' \cos\theta - \theta'^2 \sin\theta]\hat{\boldsymbol{x}} - [\zeta'^2 \cos\theta + \theta'' \sin\theta + \theta'^2 \cos\theta]\hat{\boldsymbol{t}} \\ &\quad + [\zeta'' \cos\theta - 2\theta'\zeta' \sin\theta]\hat{\boldsymbol{t}} \times \hat{\boldsymbol{x}}.\end{aligned} \tag{H5}$$

Comparing this expression with the Euler-Lagrange equation (H3), this must also equal

$$\frac{1}{K}[\mu(x)\hat{\boldsymbol{n}} - gn_x\hat{\boldsymbol{x}}] = \frac{\mu - g}{K}\sin\theta\hat{\boldsymbol{x}} + \frac{\mu}{K}\cos\theta\hat{\boldsymbol{t}}. \tag{H6}$$

Equating the $\hat{\boldsymbol{x}}$ components of these two expressions enables us to solve for the Lagrange multiplier $\mu(x)$:

$$\mu(x) = K[\theta'' \cot\theta - \theta'^2] + g. \tag{H7}$$

From the $\hat{\boldsymbol{t}} \times \hat{\boldsymbol{x}}$ components of (H5) and (H6) we immediately obtain

$$\zeta'' \cos\theta = 2\theta'\zeta' \sin\theta, \tag{H8}$$

which can be reorganized as

$$\frac{\zeta''}{\zeta'} = \frac{2\theta' \sin\theta}{\cos\theta}. \tag{H9}$$

The left-hand side of this expression is $\frac{d\ln\zeta'}{dx}$, while the right-hand side is $-2\frac{d\ln\cos\theta}{dx}$. Hence this equation can be rewritten as

$$\frac{d}{dx}[\ln(\zeta' \cos^2\theta)] = 0 \tag{H10}$$

or

$$\zeta' = C\sec^2\theta, \tag{H11}$$

where C is a constant of integration that can be fixed by the boundary conditions, which, taken together with Eq. (H11), imply $\zeta_0 = C\int_{-L/2}^{L/2} \sec^2\theta\, dx$.

From the $\hat{\boldsymbol{t}}$ component of (H6) we obtain, using (H7) and (H11),

$$-K[C^2 \sec^3\theta + \theta'' \sin\theta + \theta'^2 \cos\theta] = (K[\theta'' \cot\theta - \theta'^2] + g)\cos\theta, \tag{H12}$$

which can be solved for θ'':

$$\theta'' = -C^2 \sec^3\theta \sin\theta - \frac{g}{K}\sin\theta\cos\theta. \tag{H13}$$

The first integral of this gives

$$\theta'^2 = \frac{g}{K}(\sin^2\theta_0 - \sin^2\theta) + C^2(\sec^2\theta_0 - \sec^2\theta), \tag{H14}$$

where θ_0 is the maximum value taken by θ. Equation (H14) can be solved analytically in closed form

$$\frac{\sin\theta}{\sin\theta_0} = \mathrm{sn}\left[\left(x + \frac{L}{2}\right)\sqrt{\frac{g}{K} + C^2\sec^2\theta_0}\,\middle|\,\frac{g\sin^2\theta_0}{g + KC^2\sec^2\theta_0}\right], \tag{H15}$$

where $\mathrm{sn}[z|m]$ is the Jacobi elliptic function with elliptic modulus m. It is more informative, however, to look at the $\theta_0 \ll 1$ limit of the derivative of (H14), which is

$$\theta'' + \theta\left(\frac{g}{K} + C^2\right) - \frac{2}{3}\theta^3\left(\frac{g}{K} - 2C^2\right) = 0. \tag{H16}$$

This is recognizable as Duffing's equation; its solution can be expanded [54] in the small parameter $\epsilon \equiv -\theta_0^2(2g/K - 4C^2)/(3g/K + 3C^2)$ as

$$\frac{\theta[t(x)]}{\theta_0} = \cos t + \epsilon\left[\frac{1}{32}(\cos 3t - \cos t) - \frac{3}{8}t\sin t\right] + O(\epsilon^2), \tag{H17}$$

where we have defined $t(x) \equiv x\sqrt{g/K + C^2}$ for reasons that we now explain. Duffing's equation can be used to approximate a planar pendulum for which the period is $T = 2\pi(1 - 3\epsilon/8) + O(\epsilon^2)$. In our case, in order to satisfy the boundary condition $\theta(\pm L/2) = 0$ (with the maximum attained at $x = 0$) we require $t(L/2) = T/4$ or

$$\frac{L}{2}\sqrt{\frac{g}{K} + C^2} = \frac{\pi}{2}\left(1 - \frac{3}{8}\epsilon\right). \tag{H18}$$

Close to the Frederiks transition, where the field is just above its critical value g_c, $\theta(x) = \theta_0\cos(\pi x/L) + O(\epsilon)$, and to leading order the boundary condition on ζ is therefore $\zeta_0 = LC(1 + \theta_0^2/2)$. When $g = g_c$, the critical value of the field, Eq. (H18) is satisfied with $\theta_0 = 0$, in which case $C = \zeta_0/L$ and $\epsilon = 0$, allowing us to conclude that

$$g_c = \frac{K}{L^2}\left(\pi^2 - \zeta_0^2\right). \tag{H19}$$

Then writing $g = g_c + \Delta g$ and expanding Eq. (H18) to first order in the small quantities $\Delta g L^2/K$ and θ_0^2, we can now relate the maximum amplitude θ_0 to the incremental field Δg:

$$\theta_0^2 = \frac{2\Delta g L^2}{K\left(\pi^2 - \zeta_0^2\right)}. \tag{H20}$$

APPENDIX I: LIVING LIQUID CRYSTALS

These systems are a mixture of living bacteria, which provide the activity, and a background medium composed of nematically ordered nonactive molecules. That such a system is an active nematic can be seen on symmetry grounds: The symmetry is that of a nematic and the bacteria are active. Hence, the composite system as a whole is an active nematic and since the hydrodynamic equations are, as always, determined by symmetry (and the fact that the system is active), the hydrodynamic equations will be those we have considered here, except for one detail: Living liquid crystals are a mixture of two components (i.e., bacteria and background liquid crystal) and each component is separately conserved (assuming we neglect birth and death of the bacteria, which is frequently but not always the case; see [55]). Hence, there is one more conserved variable in this two-component active nematic and, as usual in hydrodynamics [56], conserved quantities are hydrodynamic variables. So the two-component active nematic has one more hydrodynamic variable

than the one-component active nematic that we have considered throughout the rest of this paper, which, of course, changes the hydrodynamics. We can take this extra hydrodynamic variable to be the concentration $c(\boldsymbol{r},t)$ of bacteria. The detailed effects of this modification of the hydrodynamics are not addressed in this paper. Here we limit ourselves to the observation that the hydrodynamic equations are sufficiently similar in that case that the criterion $\nabla \times \boldsymbol{f}_a \neq \boldsymbol{0}$ for thresholdless flow, described in detail after Eq. (1), is unchanged. Here we assume that in the composite system, frequent reversals in the direction of bacterial flow occur; however, note that if these reversals are rare, then different behavior may arise.

[1] M. C. Marchetti, J. F. Joanny, S. Ramaswamy, T. B. Liverpool, J. Prost, M. Rao, and R. A. Simha, Hydrodynamics of soft active matter, Rev. Mod. Phys. **85**, 1143 (2013).

[2] R. Voituriez, J. F. Joanny, and J. Prost, Spontaneous flow transition in active polar gels, Europhys. Lett. **70**, 404 (2005).

[3] K. Kruse, J. F. Joanny, F. Jlicher, J. Prost, and K. Sekimoto, Generic theory of active polar gels: A paradigm for cytoskeletal dynamics, Eur. Phys. J. E **16**, 5 (2005).

[4] W. F. Paxton, P. T. Bake, T. R. Kline, Y. Wang, T. E. Mallouk, and A. Sen, Catalytically induced electrokinetics for motors and micropumps, J. Am. Chem. Soc. **128**, 14881 (2006).

[5] C. W. Reynolds, Flocks, herds and schools: A distributed behavioral model, Comput. Graph. **21**, 25 (1987).

[6] J. L. Deneubourg and S. Goss, Collective patterns and decision-making, Ethol. Ecol. Evol. **1**, 295 (1989).

[7] A. Huth and C. Wissel, The movement of fish schools: a simulation model, in *Biological Motion*, Lecture Notes in Biomathematics, edited by W. Alt and G. Hoffmann (Springer, Berlin, 1990).

[8] B. L. Partridge, The structure and function of fish schools, Sci. Am. **246**, 114 (1982).

[9] K. Tunstrom, Y. Katz, C. C. Ioannou, C. Huepe, M. Lutz, and I. D. Couzin, Collective states, multistability and transitional behavior in schooling fish, PLoS Comput. Biol. **9**, 1002915 (2013).

[10] W. Loomis, *The Development of Dictyostelium discoideum* (Academic, New York, 1982).

[11] J. T. Bonner, *The Cellular Slime Molds* (Princeton University Press, Princeton, 1967).

[12] A. Attanasi, A. Cavagna, L. Del Castello, I. Giardina, S. Melillo, L. Parisi, O. Pohl, B. Rossaro, E. Shen, E. Silvestri, and M. Viale, Collective behavior without collective order in wild swarms of midges, PLoS Comput. Biol. **10**, 1 (2014).

[13] S. Zhou, A. Sokolov, O. D. Lavrentovich, and I. S. Aranson, Living liquid crystals, Proc. Natl. Acad. Sci. USA **111**, 1265 (2014).

[14] J. Toner and Y. Tu, Long-Range Order in a Two-Dimensional Dynamical XY Model: How Birds Fly Together, Phys. Rev. Lett. **75**, 4326 (1995).

[15] Y. Tu, J. Toner, and M. Ulm, Sound Waves and the Absence of Galilean Invariance in Flocks, Phys. Rev. Lett. **80**, 4819 (1998).

[16] J. Toner and Y. Tu, Flocks, herds, and schools: A quantitative theory of flocking, Phys. Rev. E **58**, 4828 (1998).

[17] J. Toner, Y. Tu, and S. Ramaswamy, Hydrodynamics and phases of flocks, Ann. Phys. **318**, 170 (2005).

[18] R. A. Simha and S. Ramaswamy, Hydrodynamic Fluctuations and Instabilities in Ordered Suspensions of Self-Propelled Particles, Phys. Rev. Lett. **89**, 058101 (2002).

[19] A. Souslov, B. C. van Zuiden, D. Bartolo, and V. Vitelli, Topological sound in active-liquid metamaterials, Nat. Phys. (2017), doi:10.1038/nphys4193.

[20] F. C. Keber, E. Loiseau, T. Sanchez, S. J. DeCamp, L. Giomi, M. J. Bowick, M. C. Marchetti, Z. Dogic, and A. R. Bausch, Topology and dynamics of active nematic vesicles, Science **345**, 1135 (2014).

[21] L. Giomi, M. J. Bowick, X. Ma, and M. C. Marchetti, Defect Annihilation and Proliferation in Active Nematics, Phys. Rev. Lett. **110**, 228101 (2013).

[22] L. Giomi, Geometry and Topology of Turbulence in Active Nematics, Phys. Rev. X **5**, 031003 (2015).

[23] T. Sanchez, D. T. N. Chen, S. J. DeCamp, M. Heymann, and Z. Dogic, Spontaneous motion in hierarchically assembled active matter, Nature (London) **491**, 431 (2012).

[24] M. Ravnik and J. M. Yeomans, Confined Active Nematic Flow in Cylindrical Capillaries, Phys. Rev. Lett. **110**, 026001 (2013).
[25] D. Marenduzzo, E. Orlandini, M. E. Cates, and J. M. Yeomans, Steady-state hydrodynamic instabilities of active liquid crystals: Hybrid lattice Boltzmann simulations, Phys. Rev. E **76**, 031921 (2007).
[26] L. Giomi, M. C. Marchetti, and T. B. Liverpool, Complex Spontaneous Flows and Concentration Banding in Active Polar Films, Phys. Rev. Lett. **101**, 198101 (2008).
[27] L. Giomi, L. Mahadevan, B. Chakraborty, and M. F. Hagan, Banding, excitability and chaos in active nematic suspensions, Nonlinearity **25**, 2245 (2012).
[28] S. A. Edwards and J. M. Yeomans, Spontaneous flow states in active nematics: A unified picture, Europhys. Lett. **85**, 18008 (2009).
[29] P.-G. de Gennes and J. Prost, *The Physics of Liquid Crystals* (Oxford University Press, New York, 1993).
[30] C. Peng, T. Turiv, Y. Guo, Q. Wei, and O. Lavrentovich, Command of active matter by topological defects and patterns, Science **354**, 882 (2016).
[31] F. M. Leslie, Some constitutive equations for liquid crystals, Arch. Ration. Mech. Anal. **28**, 265 (1968).
[32] N. Kuzuu and M. Doi, Constitutive equation for nematic liquid crystals under weak velocity gradient derived from a molecular kinetic equation. II. Leslie coefficients for rodlike polymers, J. Phys. Soc. Jpn. **53**, 1031 (1984).
[33] S. P. Thampi, R. Golestanian, and J. M. Yeomans, Vorticity, defects and correlations in active turbulence, Philos. Trans. R. Soc. London, Ser. A **372**, 20130366 (2014).
[34] V. Vitelli and D. R. Nelson, Nematic textures in spherical shells, Phys. Rev. E **74**, 021711 (2006).
[35] T. Lopez-Leon, V. Koning, K. B. S. Devaiah, V. Vitelli, and A. Fernandez-Nieves, Frustrated nematic order in spherical geometries, Nat. Phys. **7**, 391 (2011).
[36] A. Fernandez-Nieves, V. Vitelli, A. S. Utada, D. R. Link, M. Márquez, D. R. Nelson, and D. A. Weitz, Novel Defect Structures in Nematic Liquid Crystal Shells, Phys. Rev. Lett. **99**, 157801 (2007).
[37] R. D. Kamien, The geometry of soft materials: A primer, Rev. Mod. Phys. **74**, 953 (2002).
[38] C. D. Santangelo, V. Vitelli, R. D. Kamien, and D. R. Nelson, Geometric Theory of Columnar Phases on Curved Substrates, Phys. Rev. Lett. **99**, 017801 (2007).
[39] I. R. Kenyon, *General Relativity* (Oxford University Press, Oxford, 1990).
[40] V. Vitelli and D. R. Nelson, Defect generation and deconfinement on corrugated topographies, Phys. Rev. E **70**, 051105 (2004).
[41] M. Bowick, D. R. Nelson, and A. Travesset, Curvature-induced defect unbinding in toroidal geometries, Phys. Rev. E **69**, 041102 (2004).
[42] E. Pairam, J. Vallamkondu, V. Koning, B. C. van Zuiden, P. W. Ellis, M. A. Bates, V. Vitelli, and A. Fernandez-Nieves, Stable nematic droplets with handles, Proc. Natl. Acad. Sci. USA **110**, 9295 (2013).
[43] V. Koning, B. C. van Zuiden, R. D. Kamien, and V. Vitelli, Saddle-splay screening and chiral symmetry breaking in toroidal nematics, Soft Matter **10**, 4192 (2014).
[44] Z. S. Davidson, L. Kang, J. Jeong, T. Still, P. J. Collings, T. C. Lubensky, and A. G. Yodh, Chiral structures and defects of lyotropic chromonic liquid crystals induced by saddle-splay elasticity, Phys. Rev. E **91**, 050501 (2015).
[45] A. Sokolov, S. Zhou, O. D. Lavrentovich, and I. S. Aranson, Individual behavior and pairwise interactions between microswimmers in anisotropic liquid, Phys. Rev. E **91**, 013009 (2015).
[46] Y. Guo, M. Jiang, C. Peng, K. Sun, O. Yaroshchuk, O. Lavrentovich, and Q. H. Wei, High-resolution and high-throughput plasmonic photopatterning of complex molecular orientations in liquid crystals, Adv. Mater. **28**, 2353 (2016).
[47] See Supplemental Material at http://link.aps.org/supplemental/10.1103/PhysRevFluids.2.104201 for movies of flows in selected geometries.
[48] N. D. Mermin and H. Wagner, Absence of Ferromagnetism or Antiferromagnetism in One- or Two-Dimensional Isotropic Heisenberg Models, Phys. Rev. Lett. **17**, 1133 (1966).
[49] P. C. Hohenberg, Existence of long-range order in one and two dimensions, Phys. Rev. **158**, 383 (1967).
[50] G. P. Crawford, D. W. Allender, J. W. Doane, M Vilfan, and I. Vilfan, Finite molecular anchoring in the escaped-radial nematic configuration, Phys. Rev. A **44**, 2570 (1991).

[51] P. Guillamat, J. Igns-Mullol, and F. Sagus, Control of active liquid crystals with a magnetic field, Proc. Natl. Acad. Sci. USA **113**, 5498 (2016).
[52] J. W. Bates, On toroidal Green's functions, J. Math. Phys. **38**, 3679 (1997).
[53] A. Rotenberg, The calculation of toroidal harmonics, Math. Comput. **14**, 274 (1960).
[54] C. Bender and S. Orszag, *Advanced Methods for Scientists and Engineers* (McGraw-Hill, New York, 1978).
[55] J. Toner, Birth, Death, and Flight: A Theory of Malthusian Flocks, Phys. Rev. Lett. **108**, 088102 (2012).
[56] P. M. Chaikin and T. C. Lubensky, *Principles of Condensed Matter Physics* (Cambridge University Press, Cambridge, 1995).